
Can Biologically Plausible Temporal Credit Assignment Rules Match BPTT for Neural Similarity? E-prop as an Example

Yuhan Helena Liu^{1,2} Guangyu Robert Yang^{3,4} Christopher J. Cueva^{3,5}

Abstract

Understanding how the brain learns may be informed by studying biologically plausible learning rules. These rules, often approximating gradient descent learning to respect biological constraints such as locality, must meet two critical criteria to be considered an appropriate brain model: (1) good neuroscience task performance and (2) alignment with neural recordings. While extensive research has assessed the first criterion, the second remains underexamined. Employing methods such as Procrustes analysis on well-known neuroscience datasets, this study demonstrates the existence of a biologically plausible learning rule — namely e-prop, which is based on gradient truncation and has demonstrated versatility across a wide range of tasks — that can achieve neural data similarity comparable to Backpropagation Through Time (BPTT) when matched for task accuracy. Our findings also reveal that model architecture and initial conditions can play a more significant role in determining neural similarity than the specific learning rule. Furthermore, we observe that BPTT-trained models and their biologically plausible counterparts exhibit similar dynamical properties at comparable accuracies. These results underscore the substantial progress made in developing biologically plausible learning rules, highlighting their potential to achieve both competitive task performance and neural data similarity.

1. Introduction

Understanding how animals learn complex behaviors that span multiple temporal scales is a fundamental question in neuroscience. Effectively updating synaptic weights to achieve such learning requires solving the temporal credit assignment problem: determining how to assign the contribution of past neural states to future outcomes. In pursuit of answers, neuroscientists have increasingly adopted the mathematical framework of training recurrent neural networks (RNNs) as a model for brain learning mechanisms, inspired by seminal works that laid the foundation for this approach (Zipser, 1991; Fetz, 1992; Moody et al., 1998; Mante et al., 2013). This strategy has driven significant advancements in developing biologically plausible (bio-plausible) learning rules, which aim to model learning processes that respect biological constraints (e.g., locality (Marschall et al., 2019; Bredenberg et al., 2023)) while achieving good task performance (Lillicrap et al., 2020; Richards et al., 2019). Specifically, biological plausibility here refers to learning rules where all signals required for weight updates are physically available at the synapse (Marschall et al., 2019). Beyond synaptic-level constraints, a learning rule appropriate for the brain must also meet two key criteria: (1) it must support good task performance, and (2) it must produce brain-like activity. While extensive work has addressed the first question, the second — whether bio-plausible learning rules yield brain-like representations — remains underexamined.

Navigating the vast space of computational models — which vary not only in learning rules but also in architecture and tasks (Richards et al., 2019; Zador, 2019; Yang & Molano-Mazón, 2021) — necessitates a systematic comparison of model representations with empirical brain data. To address this challenge, a variety of methods have been developed, aiming to quantify the similarity between computational models and neural data. Among these, popular methodologies include linear regression (Yamins et al., 2014), Representational Similarity Analysis (RSA) (Kriegeskorte et al., 2008), Centered Kernel Alignment (CKA) (Kornblith et al., 2019), Singular Vector Canonical Correlation Analysis (Raghu et al., 2017), Procrustes distance (Williams et al., 2021; Ding et al., 2021; Duong et al., 2022), and Dynamical

¹Center for Statistics and Machine Learning, Princeton University, Princeton, NJ, USA ²Princeton Neuroscience Institute, Princeton University, Princeton, NJ, USA ³McGovern Institute for Brain Research, Massachusetts Institute of Technology, Cambridge, MA, USA ⁴Altera, San Francisco Bay Area, CA, USA
⁵Department of Cognitive and Psychological Sciences, Brown University, Providence, RI, USA. Correspondence to: Yuhan Helena Liu <hl7582@princeton.edu>, Christopher J. Cueva <ccueva@gmail.com>.

Proceedings of the 42nd International Conference on Machine Learning, Vancouver, Canada. PMLR 267, 2025. Copyright 2025 by the author(s).

Similarity Analysis (DSA) (Ostrow et al., 2024). By comparing the geometry of state representations or the dynamics of neural activity, these methods provide a critical framework for evaluating the extent to which models approximate neural systems.

Leveraging existing comparison methodologies, we compute the similarity scores of RNN models trained with bio-plausible learning rules to experimental data. Specifically, we evaluate these similarity scores by comparing them to those achieved by Backpropagation Through Time (BPTT)-trained models, as BPTT-trained RNNs are the predominant method for brain modeling and the benchmark that many bio-plausible learning rules aim to approximate (Yang & Wang, 2020; Richards et al., 2019; Lillicrap et al., 2020). This comparison allows us to assess the efficacy of bio-plausible approximations of gradient-descent learning in capturing neural data similarity. **Has the pursuit of biologically plausible learning rules obeyed plausibility at the level of synaptic implementation (e.g., locality) at the expense of reproducing brain-like neural activity — or can some such rules, under the right conditions, yield representations as brain-like as those learned by BPTT?**

Main contributions: Our findings reveal that the distance between data and models trained with truncation-based bio-plausible learning rules is comparable to the distance achieved by models trained using BPTT. We specifically focus on learning rules that approximate the gradient by truncating bio-impractical terms, as these truncation-based bio-plausible rules, such as e-prop, have demonstrated efficacy and versatility in learning non-trivial tasks (Bellec et al., 2020; Eyono et al., 2022). Other bio-plausible training strategies for RNNs either have limited versatility or success on non-trivial tasks (see Related Works). Specifically, our contributions include:

- We demonstrate there *exists* a biologically plausible learning rule — e-prop, which is a local learning rule based on gradient truncation and versatile across tasks — that can achieve neural data similarity comparable to BPTT at equal accuracies. We also examine ModProp in Appendix Figure 7. This is achieved by benchmarking well-known neuroscience datasets — Mante 2013 (Mante et al., 2013) and Sussillo 2015 (Sussillo et al., 2015) — which are primate datasets chosen for their higher task difficulty compared to datasets from other species, using state-of-the-art similarity methods, particularly Procrustes distance (Figure 1 and Appendix Figure 7).
- Second, we show that factors such as architecture and initial conditions — particularly initial weight settings — can have a more pronounced impact on neural data similarity than the specific choice of learning rule. This

highlights that variations in these factors can surpass differences observed across learning rules (Figure 2).

- Third, to explain the comparable similarities between BPTT and e-prop, we investigate their commonalities. We show their increased similarity at a lower learning rate for BPTT (Figure 3). We also analyze their resemblance in terms of their top demixed principal components (Figure 4), post-training weight eigenspectrum, and dynamical properties, explored via Dynamical Similarity Analysis (DSA) in Appendix Figure 8.

2. Related Works

Understanding the mechanisms through which the brain learns, utilizing its myriad elements, remains a perennial quest in neuroscience. Recent years have seen a resurgence of interest in proposing biologically plausible learning rules (Lillicrap et al., 2020; Scellier & Bengio, 2017; Hinton, 2022; Laborie & Zenke, 2022; Greedy et al., 2022; Sacramento et al., 2018; Payeur et al., 2021; Roelfsema & Holtmaat, 2018; Aljadeff et al., 2019; Meulemans et al., 2022; Murray, 2019; Bellec et al., 2020; Liu et al., 2021; 2022b; Marschall et al., 2020; Ghosh et al., 2023; Wang et al., 2024; Confavreux et al., 2024; Richards et al., 2019; Kaleb et al., 2024), suggesting potential neural algorithms that leverage known biological components. Many of these rules are grounded in experimental observations of synaptic plasticity, including STDP (Bi & Poo, 1998), differential anti-Hebbian plasticity (Xie & Seung, 1999), burst-induced plasticity (Remy & Spruston, 2007), and neuromodulated Hebbian rules shown to approximate backpropagation (Payeur et al., 2021; Aceituno et al., 2023).

Despite these advances, relatively little research has examined whether such rules — motivated by neuronal or synaptic-level constraints — give rise to brain-like activity at the circuit or network level. A separate line of work focuses on inferring learning rules directly from neural recordings (Nayebi et al., 2020; Ashwood et al., 2020; Lim et al., 2015; Kepple et al., 2021; Portes et al., 2022), aiming to reconstruct the learning mechanisms underlying synaptic plasticity. In contrast, our work does not seek to identify the brain’s actual learning rule — an especially difficult task when only post-learning data is available — but instead asks: can an existing biologically plausible rule produce neural activity aligned with empirical recordings? Our framework evaluates the outcomes of learning, using flexible post hoc comparisons that do not rely on observing the learning process itself. While this approach does not provide direct mechanistic insight, it fills a critical gap by assessing whether existing bio-plausible rules can replicate the dynamics observed in the brain. Recent work has similarly begun comparing representations learned by different types of algorithms—for example, Codol et al. (2024) ex-

plore how brain-like neural dynamics for behavioral control can emerge through reinforcement learning—providing a complementary perspective to our approach.

Our research focuses on learning rules for recurrent neural networks, which are extensively used in brain modeling (Vyas et al., 2020; Perich et al., 2021; Schuessler et al., 2020; Yang et al., 2019; Mante et al., 2013; Turner et al., 2021; Valente et al., 2021; Langdon & Engel, 2022; Barak, 2017; Song et al., 2016; Maheswaranathan et al., 2019; Yang & Molano-Mazón, 2021). This study specifically investigates local learning rules that truncate gradients, as these have shown promising results in task learning and offer versatility across various network architectures. A systematic review (Marschall et al., 2020) recognized random feedback local online (RFLO) as the only fully local (hence bio-plausible) rule. Post-review developments include e-prop, an adaptation of RFLO for non-vanilla (particularly spike-based) RNNs (Belloc et al., 2020), and MDGL (Liu et al., 2021) with its extension ModProp (Liu et al., 2022b), which further refine the gradient approximation by considering local modulatory signals (Smith et al., 2020). These rules are notable for their effectiveness in bio-plausible temporal credit assignment, matching the performance of the more traditional BPTT in many settings (Eyono et al., 2022). Our study will, therefore, concentrate on these specific learning rules due to their demonstrated efficacy and bio-plausibility. Further details of these rules are explained in Appendix A.2.

Alternative training strategies for RNNs exist, but they either face bio-plausibility issues, lack versatility across settings, or struggle to scale to complex tasks. For instance, equilibrium propagation and related rules depend on the equilibrium assumption (Scellier & Bengio, 2017; Meulemans et al., 2022); although there are architectures similar to equilibrium propagation or deep feedback control that do not make the equilibrium assumption (Gilra & Gerstner, 2017; Kaleb et al., 2024). Within truncation-based methods, the SnAP-n algorithm introduced in (Menick et al., 2020) allows customization by selecting the truncation level n . While SnAp-1 aligns closely with e-prop/RFLO, SnAp-2 and higher n require storing a triple tensor, which poses $O(N^3)$ storage demands not yet proven feasible for neural circuits. Therefore, SnAp-n ($n \geq 2$) remains biologically implausible, while SnAp-1 effectively reduces to e-prop/RFLO under certain conditions. Beyond truncation, the KeRNL algorithm approximates long-term dependencies using first-order low-pass filters and updates parameters via node perturbation, yet this also challenges biological plausibility by requiring frequent meta-parameter updates. Other strategies like FORCE learning (Sussillo & Abbott, 2009) offer alternatives, but our scope assumes recurrent weight adjustment and the non-reservoir version faces issues with locality (Marschall et al., 2019; Bredenberg et al., 2023). This study focuses on supervised learning, setting

aside the broader field of reinforcement learning for future work, thus not covering certain learning rules like the one in (Miconi, 2017).

Comparing high-dimensional neural responses across different systems and contexts is crucial in neuroscience (Chung & Abbott, 2021) for assessing model quality, determining invariant neural states, and aligning brain-machine interface recordings, among other tasks (Schrimpf et al., 2018; Chaudhuri et al., 2019; Degenhart et al., 2020; Pagan et al., 2025). Among the myriad of methods developed to quantify representational dissimilarity (Yamins et al., 2014; Schrimpf et al., 2018; Kriegeskorte et al., 2008; Raghu et al., 2017; Shahbazi et al., 2021; Williams et al., 2021; Ding et al., 2021; Duong et al., 2022; Khosla & Williams, 2023; Lin & Kriegeskorte, 2023b; Pospisil et al., 2023; Nejatbakhsh et al., 2024)—such as linear regression, Canonical Correlation Analysis (CCA), Centered Kernel Alignment (CKA), Representational Similarity Analysis (RSA), shape metrics, and Riemannian distance—we focus on Procrustes distance for its ability to provide a proper metric for comparing the geometry of state representations, and because several weaknesses have been identified in other similarity measures that are, for example, biased due to high dimensionality, or may rely on low variance noise components of the data (Kornblith et al., 2019; Davari et al., 2022; Dujmović et al., 2023; Elmoznino & Bonner, 2024; Cloos et al., 2024). Additionally, we extend our investigation to include Dynamical Similarity Analysis (DSA (Ostrow et al., 2024)) in the Appendix, assessing system dynamics to complement our geometric analyses. Overall, the value of these existing measures stems from their ability to compare complex systems without fully understanding them by capturing key structures. However, this strength also poses a limitation: they focus on specific structures, and it remains uncertain whether these structures accurately capture the computational properties of interest. Therefore, developing new measures remains a crucial and intriguing endeavor (Sexton & Love, 2022; Sucholutsky et al., 2023; Lin & Kriegeskorte, 2023a; Klabunde et al., 2023; Bowers et al., 2023; Lampinen et al., 2024).

3. Preliminaries

3.1. RNN Training Setup

Our RNN architecture consists of N_{in} input units, N hidden units, and N_{out} readout units. The update mechanism for the hidden state at time t , $h_t \in \mathbb{R}^N$, follows the equation:

$$h_{t+1} = \beta h_t + (1 - \beta)(W_h f(h_t) + W_x x_t), \quad (1)$$

where $\beta = 1 - \frac{dt}{\tau_m} \in \mathbb{R}$ is the leak factor determined by the simulation time step dt and membrane time constant τ_m ; $f(\cdot) : \mathbb{R}^N \rightarrow \mathbb{R}^N$ represents the activation function (We used tanh to mimic type-1 neuronal firing and avoid negative firing rates but also explored ReLU activa-

tion, as shown in Appendix Figure 7); $W_h \in \mathbb{R}^{N \times N}$ and $W_x \in \mathbb{R}^{N \times N_{in}}$ are the recurrent and input weight matrices, respectively; and $x_t \in \mathbb{R}^{N_{in}}$ is the input at time t . The readout, $\hat{y}_t \in \mathbb{R}^{N_{out}}$, is calculated as a linear combination of the hidden state's activation, $f(h_t)$, with the readout weights $w \in \mathbb{R}^{N_{out} \times N}$.

To train this RNN for the specific tasks in the datasets, we used synthetic input and target output detailed in Appendix A.2. Our objective is to minimize the scalar loss $L \in \mathbb{R}$. For loss minimization, we examine various learning rules, including BPTT (our benchmark) that computes the exact gradient, $\nabla_W L(W_h) \in \mathbb{R}^{N \times (N_{in} + N + N_{out})}$, as well as bio-plausible learning rules that apply approximate gradients, $\tilde{\nabla}_W L(W) \in \mathbb{R}^{N \times (N_{in} + N + N_{out})}$:

$$\Delta W = -\eta \nabla_W L(W), \quad (2)$$

$$\widehat{\Delta W} = -\eta \tilde{\nabla}_W L(W), \quad (3)$$

where $W = [W_x \quad W_h \quad w^T] \in \mathbb{R}^{N \times (N_{in} + N + N_{out})}$ and $\eta \in \mathbb{R}$ is the learning rate.

The learning rules investigated in this study are elaborated upon in Appendix A.2. Our analysis centers on how training RNNs with different algorithms influences their similarity to neural data. Predominantly, we concentrate on the truncation-based, bio-plausible rule known as e-prop (Bellec et al., 2020), which simplifies the gradient by retaining only those terms that align with a three-factor learning rule. This includes a Hebbian eligibility trace modulated by a top-down instructive factor, potentially attributable to neuromodulators (Magee & Grienberger, 2020; Gerstner et al., 2018). It is noteworthy that e-prop is equivalent to the RFLO learning rule introduced in (Murray, 2019) under most conditions. Additionally, we explore ModProp (Liu et al., 2022b), which incorporates cell-type-specific local modulatory signals (Smith et al., 2020) to recover terms omitted by e-prop. However, due to ModProp's limitations (constrained to the adherence of Dale's law and employing the *ReLU* activation function), our examination of this rule is restricted to such specific contexts in Appendix Figure 7.

3.2. Similarity Measures

As mentioned in the Introduction, we utilize the metric Procrustes distance (Williams et al., 2021) to quantify the similarity between the hidden states of RNN models, denoted by $H \in \mathbb{R}^{B*T \times N}$, and the experimentally recorded neural responses, represented as $\tilde{H} \in \mathbb{R}^{B*T \times N'}$. Here, B represents the number of trials or experimental conditions, T denotes the number of time steps in each trial, and N and N' correspond to the number of RNN hidden units and recorded neurons, respectively. The metric Procrustes distance can be viewed as the residual distance after the two neural representations are aligned with an optimal rotation,

and is quantified as

$$\theta(H, \tilde{H}) = \min_{Q \in \mathcal{O}} \arccos \left(\frac{\langle H^\phi, \tilde{H}^\phi Q \rangle}{\|H^\phi\| \|\tilde{H}^\phi\|} \right) \quad (4)$$

where \mathcal{O} is the group of orthogonal linear transformations (Ding et al., 2021; Harvey et al., 2023).

4. Results

In our study, we analyze the similarity between task-trained RNN models and two neural datasets: Sussillo 2015 (Sussillo et al., 2015) and Mante 2013 (Mante et al., 2013). An overview of our pipeline is provided in Figure 1A, with detailed information about our RNN model setup, similarity measure, and datasets in Appendix A. We examine the similarity of RNN models, across different learning rules, to neural data, leveraging Procrustes analysis. Figure 1B shows that multiple learning rules, specifically BPTT and its truncation-based biologically plausible alternative (e-prop), achieve similar Procrustes distances from neural data across two distinct tasks: Sussillo 2015 (Sussillo et al., 2015) and Mante 2013 (Mante et al., 2013). Although the error bars for BPTT and e-prop do not appear to overlap near perfect accuracy in the Sussillo 2015 task, we demonstrate that such differences are minimal compared to other potential confounding factors in the brain, as shown in Figure 2 and Appendix Figure 7. We further demonstrate the key trend using additional similarity measures in Table 2.

Also, to see if the progress over time in developing more biologically plausible learning rules has led to improvements in aligning models with neural activity, we also evaluated older learning methods such as node perturbation and evolutionary strategies. Results show that these methods resulted in greater Procrustes distances compared to the aforementioned rules at equivalent accuracy levels, demonstrating that not all learning rules are equally effective. This also indicates the effectiveness of newer bio-plausible gradient-approximating learning rules over some of the older methods (Appendix Figure 9).

Additionally, Figure 2 delves into the impact of initial weight settings on model-data distances, revealing that such initial condition nuances exert a more pronounced influence than the choice of learning rule itself. Initial weight gain is a crucial attribute, as it significantly affects the dynamical properties of RNNs, particularly the Lyapunov exponents that govern the rates of expansion and contraction. It can also interpolate between rich and lazy learning regimes, imparting distinct inductive biases (Braun et al., 2022; Flesch et al., 2023; Chizat et al., 2019; Woodworth et al., 2020; Schuessler et al., 2023; Bordelon & Pehlevan, 2022; Liu et al., 2023; Paccolat et al., 2021). This finding further underscores the significant role of model initialization in

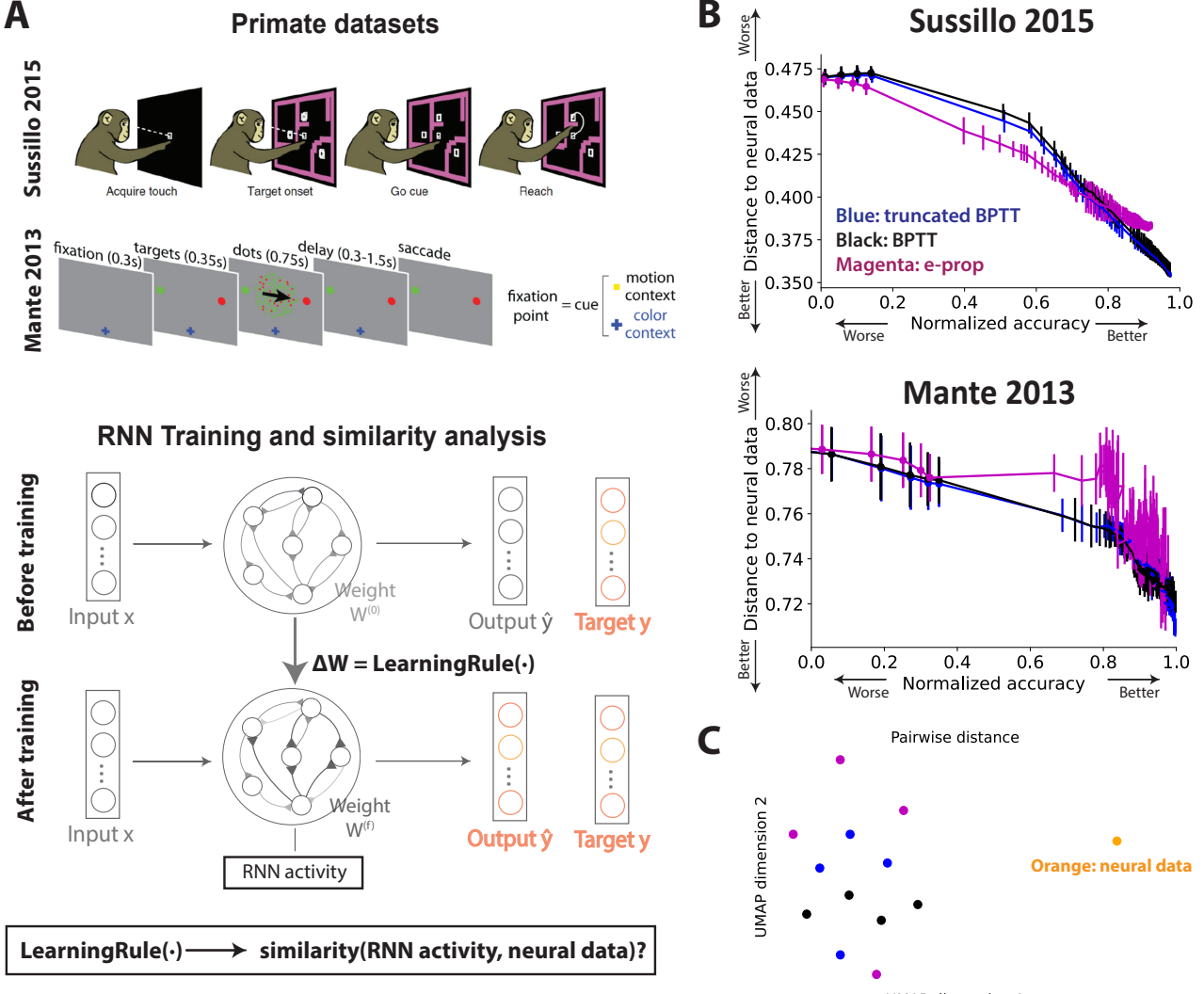


Figure 1. (A) Setup overview: analysis of two neural datasets. We computed similarity scores between RNN activity and electrode recordings from (1) Mante et al. (2013) and (2) Sussillo et al. (2015). Schematics have been modified from those in the original papers. RNNs are trained on these respective tasks using various learning rules, including BPTT and bio-plausible alternatives. Subsequently, we evaluate the similarity between RNN activity post-training and the neural recordings to compare model-data similarity across different learning rules. (B) The Procrustes distance vs. accuracy plots for the Sussillo 2015 (top) and Mante 2013 (bottom) tasks illustrate that multiple learning rules achieve comparable data similarity. At each training iteration, both task accuracy and neural similarity are computed, and the resulting pairs are plotted—showing the progression of models during training from low accuracy/high distance (upper left) to high accuracy/low distance (bottom right). This procedure is applied uniformly across all learning rules. Here, magenta denotes e-prop, blue denotes truncated BPTT (truncation length = 10), and black denotes BPTT. The mean is plotted with error bars denoting standard deviations across four random seeds. The x-axis, normalized accuracy, is defined in Appendix A.3. (C) UMAP embedding of trained model representations with Sussillo 2015 as an illustrative example; additional training snapshots are shown in Appendix Figure 6. Additional similarity measures are given in Table 2.

shaping learning outcomes, with particular initial conditions facilitating a closer approximation to neural data than others.

Figure 3 explores the impact of learning rates on model-data distances across learning rules. In Figure 3A, Procrustes distances remain consistent across learning rates for BPTT.

Given that e-prop can be decomposed into a lower learning rate BPTT and an approximation error (Liu et al., 2022a), which is further illustrated here by the similarity between a lower learning rate BPTT and e-prop (Figure 3B), this shared component of a lower learning rate BPTT could partly explain their similar distances. Additionally, post-

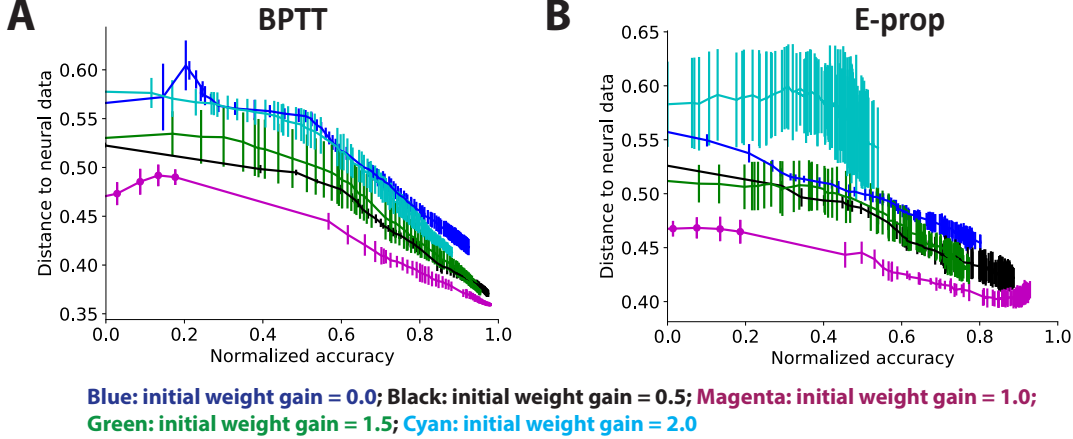


Figure 2. Impact of Initial Weight Magnitude on Model-Data Distances Exceeds Variation from Learning Rules. Model-data distances versus normalized accuracy for various initial gain values (depicted by different colors) for (A) BPTT and (B) e-prop. Initial weight gain refers to the multiplier applied to the default initializations for recurrent and readout weights. The results shown are for the Sussillo 2015 task, with similar trends observed for the Mante 2013 task. The mean is plotted with error bars representing the standard deviation. Table 1 further illustrates the significant influence of gain on distances.

Rule	gain=0.0	gain=0.5	gain=1.0	gain=1.5	1.0 vs 0.0	1.0 vs 0.5
BPTT	0.461 ± 0.006	0.423 ± 0.005	0.398 ± 0.007	0.428 ± 0.010	$p=2.07e-5$	$p=1.94e-3$
e-prop	0.461 ± 0.007	0.437 ± 0.009	0.407 ± 0.008	0.432 ± 0.008	$p=1.30e-4$	$p=5.71e-3$
e-prop vs BPTT	$p=0.985$	$p=0.078$	$p=0.173$	$p=0.587$	—	—
Noise ceiling	0.565 ± 0.002	0.529 ± 0.005	0.467 ± 0.005	0.508 ± 0.017	—	—

Table 1. Procrustes distance across gains and learning rules for Figure 2. Distances measured at normalized accuracy ≈ 0.8 . Values are mean \pm std across seeds. Noise ceiling corresponds to untrained models. Non-overlapping error bars across gains suggest gain influences neural distances; overlapping bars within columns suggest similarity across rules (for fixed gain). P-values (uncorrected t-tests due to only a small number of comparisons) highlight significant gain-dependent differences but insignificant differences across rules.

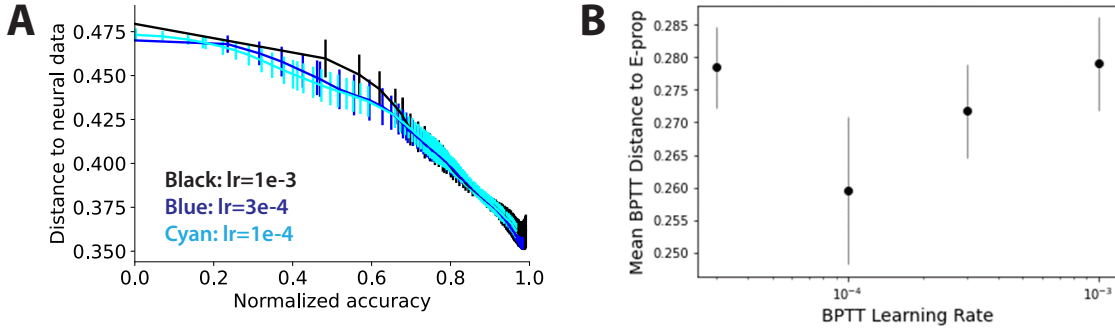


Figure 3. (A) Procrustes distances remain consistent across various learning rates when employing the same rule (BPTT). Different color shades represent different learning rates: $1e-3$, $3e-4$, and $1e-4$. These rates result in nearly indistinguishable Procrustes distances. The analysis in this figure is done using the Sussillo 2015 task. (B) E-prop — has been viewed as BPTT with a reduced learning rate plus some degree of gradient approximation error (Liu et al., 2022a) — aligns more closely with BPTT at a lower learning rate ($1e-4$) compared to the default setting ($1e-3$). Here, the mean distance from BPTT to e-prop is plotted, with error bars denoting the standard deviation.

training weight eigenspectrums and distances, analyzed via Dynamical Similarity Analysis (DSA), further reinforce the similarity between BPTT and e-prop (Appendix Figure 8).

This similarity is further explored in Figure 4, where top demixed principal components show a qualitative match between the neural data and the models. We also display the

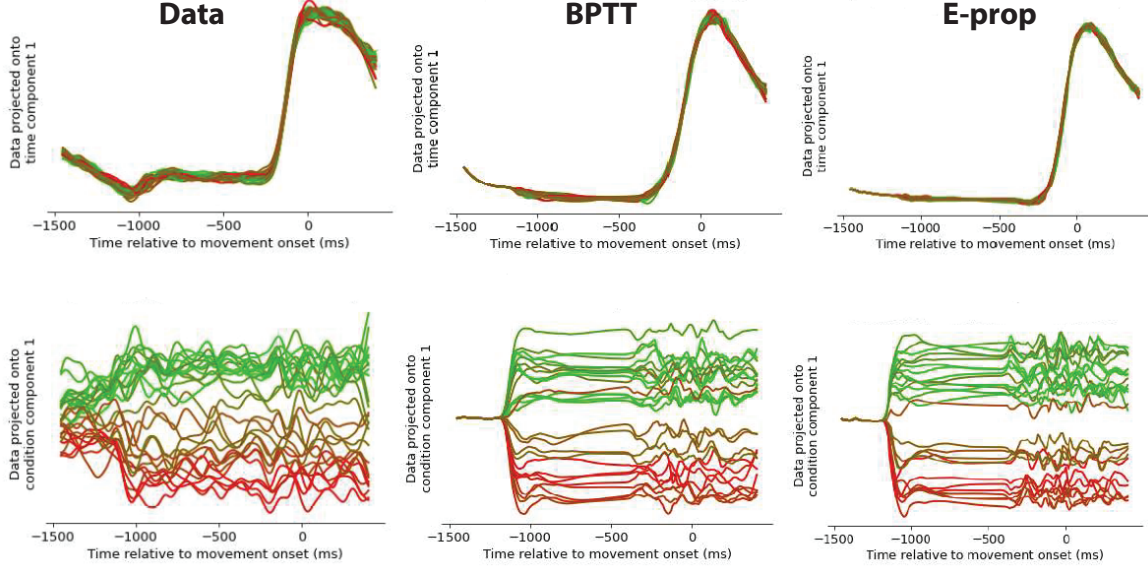


Figure 4. Demixed principal component analysis (dPCA) shows a qualitative match between model and data when projected onto the first time component and first condition component. The time component captures variance aligned with task time, while the condition component captures variance attributable to input condition differences. Here, the Sussillo 2015 dataset is illustrated; similar trends are observed for the Mante 2013 dataset. Each color represents a different reach condition.

	CCA	CKA
BPTT	0.272 ± 0.009	0.152 ± 0.015
e-prop	0.273 ± 0.009	0.154 ± 0.006
p-val	$p=0.953$	$p=0.817$

Table 2. Additional similarity measures yield trends consistent with those in Figure 1. We note that Sussillo 2015 is used here as an example. All p-values (uncorrected, due to the small number of comparisons) show no significant differences between trained BPTT and e-prop models across metrics (at matched accuracies).

similarity among models in terms of their pairwise distances and their embeddings across different sampled training snapshots in Appendix Figure 6.

Building on the observed similarities between BPTT and e-prop, we derive Proposition 4.1, which demonstrates that e-prop can converge to W^* (the solution obtained by BPTT) in a highly simplified setting, highlighting the critical role of initialization. Specifically, we present a 1D linear RNN example where e-prop matches BPTT under certain initializations but diverges under others. This toy case illustrates the sensitivity of e-prop to initialization, a key factor also observed in our empirical results. Extending such theoretical analysis to higher-dimensional RNNs would be valuable, though likely on the order of (Schuessler et al., 2020), and is left for future work. Our aim is not to offer a comprehensive theoretical account of e-prop, but rather to motivate future investigation by showing that convergence behavior in even

the simplest cases can depend strongly on initialization.

Proposition 4.1. *(Informal)* For a 1D linear RNN trained using e-prop, the weight updates can converge to (or diverge from) the solution W^* found via an arbitrary algorithm (e.g., BPTT), depending on the initialization of the recurrent weight $W(0)$. *(The formal statement and proof are provided in Appendix B.)*

It is noteworthy that if all models were equally far from the data, it might also suggest random noise. However, that is not the case, as our models are significantly closer to the neural data after training (Figure 5 and Table 3). These results are also consistent with the existing studies that reported the correlation between task performance and neural data similarity (Yamins et al., 2014). Additionally, what does it mean for a model to be close to the data and how do we interpret the range of alignment values? To interpret those, we need a baseline based on data-to-data similarity, which reflects how close the models are to the data relative to other data points (subsamples within the dataset). Due to limited subjects, we generated this baseline by splitting the data by neurons within the same subject, matched across timepoints and experimental conditions, though this may create an overly stringent baseline due to potential neuron dependence (details in Appendix A.3). We also explain why we didn't use trial-based subsampling in Appendix A.3. For the Hatsopoulos 2007 dataset (Hatsopoulos et al., 2007), the final trained models match the neural data as closely as other neurons (Figure 5). For the Sussillo 2015 and Mante 2013

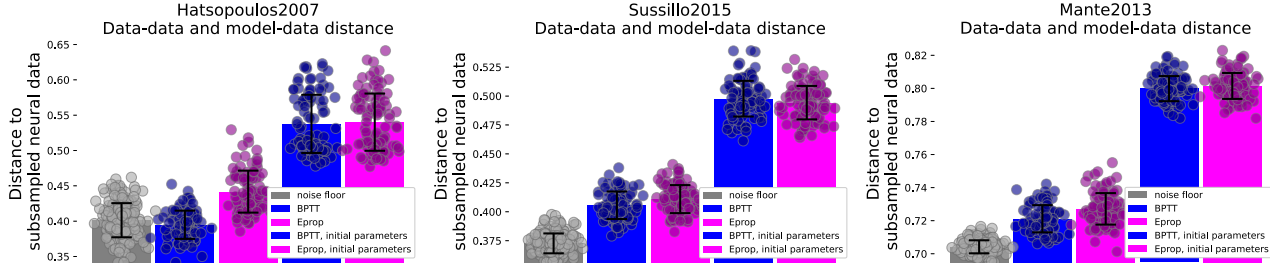


Figure 5. Data-to-data distance (noise floor) vs model-to-data distance (BPTT and e-prop before and after training). Left: Hatsopoulos 2007; middle: Sussillo 2015; right: Mante 2013. The data-splitting procedure for obtaining the baseline (i.e. noise floor) is detailed in Appendix A.3. We also tabularize these values in Table 3. We note that these distances are computed with fewer neurons (about half) and units than the previous plots, so the exact distance values here may differ.

Dataset	Noise floor	BPTT (trained)	e-prop (trained)	Untrained	BPTT vs. floor
Hatsopoulos 2007	0.401 ± 0.024	0.395 ± 0.020	0.442 ± 0.030	0.538 ± 0.041	$p=0.311$
Sussillo 2015	0.373 ± 0.009	0.406 ± 0.012	0.411 ± 0.012	0.498 ± 0.015	$p=5.02e-6$
Mante 2013	0.704 ± 0.004	0.721 ± 0.008	0.727 ± 0.010	0.800 ± 0.008	$p=1.29e-5$

Table 3. Neural similarity scores from Figure 5. Trained models outperform their untrained initializations and the noise floor. P-values (uncorrected t-tests) compare BPTT-trained models to the noise floor; similar trend was observed for e-prop trained model as well. Significant differences from the noise floor are found for Sussillo 2015 and Mante 2013, but not for Hatsopoulos 2007.

datasets, trained models approach the noise floor compared to untrained models; the remaining differences from the baseline offer insights for improving learning algorithms and architectures in future work.

5. Discussion

Investigating biologically plausible learning rules is important to understanding how the brain learns. While many such rules adhere to synaptic-level constraints (Richards et al., 2019; Lillicrap et al., 2020), their ability to reproduce brain-like neural activity remains unclear. Here, we assess whether RNNs trained with approximate, gradient-based bio-plausible rules — focusing on e-prop (and ModProp in the Appendix) — can match the neural similarity of standard BPTT-trained models. Using Procrustes analysis, we show that at matched task accuracy, e-prop-trained RNNs exhibit neural similarity comparable to BPTT. Notably, architectural choices and initialization have a larger influence on model-data alignment than the choice of learning rule (Figure 2, Appendix Figure 7). Further, BPTT exhibits increased similarity to bio-plausible models at lower learning rates (Figure 3) and shares post-training properties in weight eigenspectrum and dynamics, as shown via DSA (Appendix Figure 8). These findings demonstrate that bio-plausible rules can, under certain conditions, achieve both strong task performance and brain-like dynamics — motivating a broader reevaluation of how architecture and initialization shape neural similarity.

While BPTT exhibits questionable biological plausibility, it has been widely used for brain modeling, especially in seminal works (Mante et al., 2013; Sussillo et al., 2015; Yamins et al., 2014; Yang & Wang, 2020). Comparing BPTT to e-prop allows us to examine how biologically motivated gradient truncation affects neural similarity, and whether BPTT-based models, despite their widespread use, might under- or overestimate representational alignment relative to plausible alternatives. Importantly, it was not obvious a priori whether e-prop would yield representations more or less brain-like than BPTT. Our finding that e-prop can match BPTT under certain conditions is therefore nontrivial and highlights the promise of such rules. More broadly, our framework is designed to eventually evaluate models that surpass BPTT as a benchmark for neural similarity.

Limitations and future works. Extending our approach to include a broader range of learning rules, architectures, datasets, and comparison methods represents an important direction for future research. A comprehensive evaluation across these dimensions is beyond the scope of a single paper, especially in a rapidly evolving field. Our pipeline is flexible, allowing for expansion across these various facets in future investigations. Moreover, while our study is limited in the learning rules and architectures examined, it demonstrates the existence of scenarios where biologically plausible learning rules can achieve neural data similarities comparable to their deep learning counterparts. Our focus on gradient truncation-based learning rules is due to their effectiveness in task learning and versatility (see Re-

lated Works). Despite focusing primarily on e-prop (and ModProp in the Appendix), our findings suggest that it’s possible for biologically plausible learning approximations to preserve synaptic-level constraints without substantially sacrificing neural data alignment. That said, existing findings do not suggest that maintaining similarity at the synaptic level necessarily translates to similarity at the neural activity level, possibly due to differences in scale and the emergent nature of neural dynamics. Additionally, while this work emphasizes learning via synaptic credit assignment, alternative frameworks such as biologically plausible in-context learning (Von Oswald et al., 2023) offer complementary perspectives and merit deeper investigation.

Another limitation worth noting is that our pipeline is not designed to identify the brain’s actual learning rule. This stems from identifiability issues inherent in under-constrained systems: multiple learning rules may converge to similar terminal activity patterns when only post-learning data are available. Constraining the architecture using experimental data — or incorporating neural data during learning — could help narrow the solution space, and we view this as a promising direction for future work. That said, our goal is not to recover the precise rule used by the brain, but rather to test whether any existing biologically plausible rule (e.g., e-prop) can yield neural dynamics comparable to those trained with BPTT, the de facto benchmark for brain-like models. Our findings suggest that such rules can indeed achieve competitive neural similarity and task performance without sacrificing biological plausibility.

Beyond learning rules, factors such as architecture and initialization — highlighted in Figure 2 and Appendix Figure 7 — are critical areas for future exploration. While our results show that e-prop can match BPTT in neural similarity at equal task accuracy, this does not imply the two are functionally indistinguishable. In fact, e-prop struggles on certain tasks (Liu et al., 2021), motivating future efforts to gather experimental data where bio-plausible rules diverge, enabling more targeted comparisons. This consideration partly motivated our focus on primate datasets, which typically involve more complex tasks than those used during rodent experiments. Expanding the analysis to more open-source primate datasets and other modalities is an important next step. Relatedly, our study centers on temporal tasks with rich dynamics, aligning with our goal of investigating biologically plausible credit assignment over time. That said, extending these analyses to non-temporal domains — such as vision, where many recent bio-plausible rules are formulated — is a valuable direction for future work.

As recent studies have noted, BPTT-trained models often converge to a limited subset of solutions (Pagan et al., 2025), and it remains unclear whether the brain uses BPTT at all (Song et al., 2024); Zahorodnii et al. (2025) further

demonstrate that handcrafted solutions can produce more brain-like dynamics than BPTT. These observations underscore the limitations of BPTT as a benchmark and motivate future research on alternative learning frameworks and rule–architecture co-design. While in our study we intentionally fixed the architecture, initialization, and task — following prior work (e.g., (Liu et al., 2022a)) — to isolate the effect of the learning rule on neural similarity, many biologically plausible rules are designed with specific architectural constraints in mind. A more systematic investigation of learning rule and architecture interactions is an important direction for future work.

Furthermore, we chose to focus on Procrustes distance for its ability to provide a proper metric for comparing the geometry of state representations, and its stringency in only allowing for rotations and a global stretching to align neural trajectories (although we also explored additional measures in Table 2 and Appendix Figure 8B). Beyond its geometric grounding, recent work (Cloos et al., 2024) found that optimizing Procrustes may better preserve task-relevant features than other metrics, suggesting it can capture more meaningful neural structure. They also showed that Procrustes is stricter than CKA: high Procrustes was observed to imply high CKA, but not vice versa (see also Harvey et al. (2024)). We were also motivated to emphasize Procrustes distance because several weaknesses have been identified in other similarity measures that are, for example, biased due to high dimensionality, or may rely on low variance noise components of the data (Kornblith et al., 2019; Davari et al., 2022; Dujimović et al., 2023; Elmoznino & Bonner, 2024; Cloos et al., 2024). That said, like all scalar measures, it focuses on specific structures, and it remains uncertain whether these structures accurately capture the computational properties of interest. Relatedly, certain deep learning architectures, under sufficient conditions, may lead many models to exhibit similar internal representations (Huh et al., 2024). Therefore, developing new measures remains a crucial and intriguing endeavor (Sexton & Love, 2022; Sucholutsky et al., 2023; Lin & Kriegeskorte, 2023a; Klabunde et al., 2023; Bowers et al., 2023; Lampinen et al., 2024). Altogether, this vibrant area invites further work on learning rule–architecture interactions, task design, and evaluation methods.

Acknowledgement

We are grateful to Mante, Hatsopoulos, and Churchland for sharing their neural datasets. We also thank Nathan Cloos and Kathryn Zhou for their preprocessing code for the Mante 2013 dataset, which builds on Valerio Mante’s original scripts. This research was supported by FRQNT B3X (Y.H.L.); Pearson Fellowship (Y.H.L.).

Impact Statement

This research advances our understanding of biologically plausible learning models in recurrent neural networks, with no immediate ethical or societal impacts expected. Over time, the findings could influence related fields like neuroscience and deep learning, potentially affecting society based on how these disciplines evolve.

References

- Aceituno, P. V., Farinha, M. T., Loidl, R., and Grewe, B. F. Learning cortical hierarchies with temporal hebbian updates. *Frontiers in Computational Neuroscience*, 17: 1136010, 2023.
- Aljadeff, J., D'amour, J., Field, R. E., Froemke, R. C., and Clopath, C. Cortical credit assignment by hebbian, neuromodulatory and inhibitory plasticity. *arXiv preprint arXiv:1911.00307*, 2019.
- Ashwood, Z., Roy, N. A., Bak, J. H., and Pillow, J. W. Inferring learning rules from animal decision-making. *Advances in Neural Information Processing Systems*, 33: 3442–3453, 2020.
- Barak, O. Recurrent neural networks as versatile tools of neuroscience research. *Current opinion in neurobiology*, 46:1–6, 2017.
- Bellec, G., Scherr, F., Subramoney, A., Hajek, E., Salaj, D., Legenstein, R., and Maass, W. A solution to the learning dilemma for recurrent networks of spiking neurons. *Nature communications*, 11(1):3625, 2020.
- Bi, G.-q. and Poo, M.-m. Synaptic modifications in cultured hippocampal neurons: dependence on spike timing, synaptic strength, and postsynaptic cell type. *Journal of neuroscience*, 18(24):10464–10472, 1998.
- Bordelon, B. and Pehlevan, C. The influence of learning rule on representation dynamics in wide neural networks. *arXiv preprint arXiv:2210.02157*, 2022.
- Bowers, J. S., Malhotra, G., Dujmović, M., Llera Montero, M., Tsvetkov, C., Biscione, V., Puebla, G., Adolfi, F., Hummel, J. E., Heaton, R. F., and et al. Deep problems with neural network models of human vision. *Behavioral and Brain Sciences*, 46:e385, 2023.
- Braun, L., Dominé, C., Fitzgerald, J., and Saxe, A. Exact learning dynamics of deep linear networks with prior knowledge. *Advances in Neural Information Processing Systems*, 35:6615–6629, 2022.
- Bredenberg, C., Williams, E., Savin, C., Richards, B., and Lajoie, G. Formalizing locality for normative synaptic plasticity models. *Advances in Neural Information Processing Systems*, 36:5653–5684, 2023.
- Chaudhuri, R., Gercek, B., Pandey, B., Peyrache, A., and Fiete, I. The intrinsic attractor manifold and population dynamics of a canonical cognitive circuit across waking and sleep. *Nature neuroscience*, 22(9):1512–1520, 2019.
- Chizat, L., Oyallon, E., and Bach, F. On lazy training in differentiable programming. *Advances in Neural Information Processing Systems*, 32, 2019.
- Chung, S. and Abbott, L. F. Neural population geometry: An approach for understanding biological and artificial neural networks. *Current opinion in neurobiology*, 70: 137–144, 2021.
- Cloos, N., Li, M., Yang, G. R., and Cueva, C. J. Scaling up the evaluation of recurrent neural network models for cognitive neuroscience. *Cognitive Computational Neuroscience*, 2022.
- Cloos, N., Li, M., Siegel, M., Brincat, S. L., Miller, E. K., Yang, G. R., and Cueva, C. J. Differentiable optimization of similarity scores between models and brains. *arXiv preprint arXiv:2407.07059*, 2024.
- Codol, O., Krishna, N. H., Lajoie, G., and Perich, M. G. Brain-like neural dynamics for behavioral control develop through reinforcement learning. *bioRxiv*, 2024.
- Confavreux, B., Ramesh, P., Goncalves, P. J., Macke, J. H., and Vogels, T. Meta-learning families of plasticity rules in recurrent spiking networks using simulation-based inference. *Advances in Neural Information Processing Systems*, 36, 2024.
- Cunningham, J. P., Gilja, V., Ryu, S. I., and Shenoy, K. V. Methods for estimating neural firing rates, and their application to brain-machine interfaces. *Neural Networks*, 22(9):1235–1246, 2009.
- Davari, M., Horoi, S., Natik, A., Lajoie, G., Wolf, G., and Belilovsky, E. Reliability of cka as a similarity measure in deep learning. *arXiv preprint arXiv:2210.16156*, 2022.
- Degenhart, A. D., Bishop, W. E., Oby, E. R., Tyler-Kabara, E. C., Chase, S. M., Batista, A. P., and Yu, B. M. Stabilization of a brain–computer interface via the alignment of low-dimensional spaces of neural activity. *Nature biomedical engineering*, 4(7):672–685, 2020.
- DePasquale, B., Cueva, C. J., Rajan, K., Escola, G. S., and Abbott, L. full-force: A target-based method for training recurrent networks. *PloS one*, 13(2):e0191527, 2018.
- Ding, F., Denain, J.-S., and Steinhardt, J. Grounding representation similarity through statistical testing. *Advances in Neural Information Processing Systems*, 34: 1556–1568, 2021.

- Dujmović, M., Bowers, J. S., Adolfi, F., and Malhotra, G. Obstacles to inferring mechanistic similarity using representational similarity analysis. *bioRxiv*, 2023.
- Duong, L. R., Zhou, J., Nassar, J., Berman, J., Olieslagers, J., and Williams, A. H. Representational dissimilarity metric spaces for stochastic neural networks. *arXiv preprint arXiv:2211.11665*, 2022.
- Elmoznino, E. and Bonner, M. F. High-performing neural network models of visual cortex benefit from high latent dimensionality. *PLOS Computational Biology*, 20(1): 1–23, 01 2024.
- Eyono, R. H., Boven, E., Ghosh, A., Pemberton, J., Scherr, F., Clopath, C., Costa, R. P., Maass, W., Richards, B. A., Savin, C., et al. Current state and future directions for learning in biological recurrent neural networks: A perspective piece. *Neurons, Behavior, Data analysis, and Theory*, 1, 2022.
- Fetz, E. Are movement parameters recognizably coded in the activity of single neurons? *Behavioral and Brain Sciences*, 15(4):679–690, 1992.
- Flesch, T., Saxe, A., and Summerfield, C. Continual task learning in natural and artificial agents. *Trends in Neurosciences*, 46(3):199–210, 2023.
- Gerstner, W., Lehmann, M., Liakoni, V., Corneil, D., and Brea, J. Eligibility Traces and Plasticity on Behavioral Time Scales: Experimental Support of NeoHebbian Three-Factor Learning Rules. *Frontiers in Neural Circuits*, 12:53, jul 2018.
- Ghosh, A., Liu, Y. H., Lajoie, G., Kording, K., and Richards, B. A. How gradient estimator variance and bias impact learning in neural networks. In *The Eleventh International Conference on Learning Representations*, 2023.
- Gilra, A. and Gerstner, W. Predicting non-linear dynamics by stable local learning in a recurrent spiking neural network. *Elife*, 6:e28295, 2017.
- Greedy, W., Zhu, H. W., Pemberton, J., Mellor, J., and Ponte Costa, R. Single-phase deep learning in cortico-cortical networks. *Advances in Neural Information Processing Systems*, 35:24213–24225, 2022.
- Harvey, S. E., Larsen, B. W., and Williams, A. H. Duality of bures and shape distances with implications for comparing neural representations. In *UniReps: the First Workshop on Unifying Representations in Neural Models*, 2023.
- Harvey, S. E., Lipshutz, D., and Williams, A. H. What representational similarity measures imply about decodable information. *arXiv preprint arXiv:2411.08197*, 2024.
- Hatsopoulos, N. G., Xu, Q., and Amit, Y. Encoding of movement fragments in the motor cortex. *Journal of Neuroscience*, 27(19):5105–5114, 2007.
- Hinton, G. The forward-forward algorithm: Some preliminary investigations. *arXiv preprint arXiv:2212.13345*, 2022.
- Huh, M., Cheung, B., Wang, T., and Isola, P. Position: The platonic representation hypothesis. In *Forty-first International Conference on Machine Learning*, 2024.
- Kaleb, K., Feulner, B., Gallego, J., and Clopath, C. Feedback control guides credit assignment in recurrent neural networks. *Advances in Neural Information Processing Systems*, 37:5122–5144, 2024.
- Kay, K., Prince, J. S., Gebhart, T., Tuckute, G., Zhou, J., Naselaris, T., and Schutt, H. Disentangling signal and noise in neural responses through generative modeling. *bioRxiv*, 2024.
- Kepple, D. R., Engelken, R., and Rajan, K. Curriculum learning as a tool to uncover learning principles in the brain. In *International Conference on Learning Representations*, 2021.
- Khosla, M. and Williams, A. H. Soft matching distance: A metric on neural representations that captures single-neuron tuning. *arXiv preprint arXiv:2311.09466*, 2023.
- Klabunde, M., Schumacher, T., Strohmaier, M., and Lemmerich, F. Similarity of neural network models: A survey of functional and representational measures. *arXiv preprint arXiv:2305.06329*, 2023.
- Kornblith, S., Norouzi, M., Lee, H., and Hinton, G. Similarity of neural network representations revisited. In *International conference on machine learning*, pp. 3519–3529. PMLR, 2019.
- Kriegeskorte, N., Mur, M., and Bandettini, P. A. Representational similarity analysis-connecting the branches of systems neuroscience. *Frontiers in systems neuroscience*, 2:249, 2008.
- Laborieux, A. and Zenke, F. Holomorphic equilibrium propagation computes exact gradients through finite size oscillations. *arXiv preprint arXiv:2209.00530*, 2022.
- Lampinen, A. K., Chan, S. C. Y., and Hermann, K. Learned feature representations are biased by complexity, learning order, position, and more. *arXiv preprint arXiv:2405.05847*, 2024.
- Langdon, C. and Engel, T. A. Latent circuit inference from heterogeneous neural responses during cognitive tasks. *bioRxiv*, 2022.

- Lillicrap, T. P., Cownden, D., Tweed, D. B., and Akerman, C. J. Random synaptic feedback weights support error backpropagation for deep learning. *Nature communications*, 7(1):1–10, 2016.
- Lillicrap, T. P., Santoro, A., Marris, L., Akerman, C. J., and Hinton, G. Backpropagation and the brain. *Nature Reviews Neuroscience*, 21(6):335–346, 2020.
- Lim, S., McKee, J. L., Woloszyn, L., Amit, Y., Freedman, D. J., Sheinberg, D. L., and Brunel, N. Inferring learning rules from distributions of firing rates in cortical neurons. *Nature neuroscience*, 18(12):1804–1810, 2015.
- Lin, B. and Kriegeskorte, N. The topology and geometry of neural representations. *arXiv preprint arXiv:2309.11028*, 2023a.
- Lin, B. and Kriegeskorte, N. The topology and geometry of neural representations. *arXiv preprint arXiv:2309.11028*, 2023b.
- Liu, Y. H., Smith, S., Mihalas, S., Shea-Brown, E., and Sümbül, U. Cell-type-specific neuromodulation guides synaptic credit assignment in a spiking neural network. *Proceedings of the National Academy of Sciences*, 118(51):e2111821118, 2021.
- Liu, Y. H., Ghosh, A., Richards, B. A., Shea-Brown, E., and Lajoie, G. Beyond accuracy: generalization properties of bio-plausible temporal credit assignment rules. *arXiv preprint arXiv:2206.00823*, 2022a.
- Liu, Y. H., Smith, S., Mihalas, S., Shea-Brown, E., and Sümbül, U. Biologically-plausible backpropagation through arbitrary timespans via local neuromodulators. *arXiv preprint arXiv:2206.01338*, 2022b.
- Liu, Y. H., Baratin, A., Cornford, J., Mihalas, S., Shea-Brown, E., and Lajoie, G. How connectivity structure shapes rich and lazy learning in neural circuits. *arXiv preprint arXiv:2310.08513*, 2023.
- Magee, J. C. and Grienberger, C. Synaptic Plasticity Forms and Functions. *Annual Review of Neuroscience*, 43(1):95–117, jul 2020.
- Maheswaranathan, N., Williams, A., Golub, M., Ganguli, S., and Sussillo, D. Universality and individuality in neural dynamics across large populations of recurrent networks. *Advances in neural information processing systems*, 32, 2019.
- Mante, V., Sussillo, D., Shenoy, K. V., and Newsome, W. T. Context-dependent computation by recurrent dynamics in prefrontal cortex. *nature*, 503(7474):78–84, 2013.
- Marschall, O., Cho, K., and Savin, C. Evaluating biological plausibility of learning algorithms the lazy way. In *Real Neurons \& Hidden Units: Future directions at the intersection of neuroscience and artificial intelligence@ NeurIPS 2019*, 2019.
- Marschall, O., Cho, K., and Savin, C. A unified framework of online learning algorithms for training recurrent neural networks. *The Journal of Machine Learning Research*, 21(1):5320–5353, 2020.
- Menick, J., Elsen, E., Evci, U., Osindero, S., Simonyan, K., and Graves, A. A practical sparse approximation for real time recurrent learning. *arXiv preprint arXiv:2006.07232*, 2020.
- Meulemans, A., Zucchet, N., Kobayashi, S., Von Oswald, J., and Sacramento, J. The least-control principle for local learning at equilibrium. *Advances in Neural Information Processing Systems*, 35:33603–33617, 2022.
- Miconi, T. Biologically plausible learning in recurrent neural networks reproduces neural dynamics observed during cognitive tasks. *Elife*, 6:e20899, 2017.
- Molano-Mazon, M., Barbosa, J., Pastor-Ciurana, J., Fradera, M., Zhang, R.-Y., Forest, J., del Pozo Lerida, J., Ji-An, L., Cueva, C. J., de la Rocha, J., et al. Neurogym: An open resource for developing and sharing neuroscience tasks. *PsyArXiv*, 2022.
- Moody, S. L., Wise, S. P., di Pellegrino, G., and Zipser, D. A model that accounts for activity in primate frontal cortex during a delayed matching-to-sample task. *Journal of Neuroscience*, 18(1):399–410, 1998.
- Murray, J. M. Local online learning in recurrent networks with random feedback. *Elife*, 8:e43299, 2019.
- Nayebi, A., Srivastava, S., Ganguli, S., and Yamins, D. L. Identifying learning rules from neural network observables. *Advances in Neural Information Processing Systems*, 33:2639–2650, 2020.
- Nejatbakhsh, A., Geadah, V., Williams, A. H., and Lipshtutz, D. Comparing noisy neural population dynamics using optimal transport distances. *arXiv preprint arXiv:2412.14421*, 2024.
- Ostrow, M., Eisen, A., Kozachkov, L., and Fiete, I. Beyond geometry: Comparing the temporal structure of computation in neural circuits with dynamical similarity analysis. *Advances in Neural Information Processing Systems*, 36, 2024.
- Paccolat, J., Petrini, L., Geiger, M., Tyloo, K., and Wyart, M. Geometric compression of invariant manifolds in neural networks. *Journal of Statistical Mechanics: Theory and Experiment*, 2021(4):044001, 2021.

- Pagan, M., Tang, V. D., Aoi, M. C., Pillow, J. W., Mante, V., Sussillo, D., and Brody, C. D. Individual variability of neural computations underlying flexible decisions. *Nature*, 639(8054):421–429, 2025.
- Pandarinath, C., O’Shea, D. J., Collins, J., Jozefowicz, R., Stavisky, S. D., Kao, J. C., Trautmann, E. M., Kaufman, M. T., Ryu, S. I., Hochberg, L. R., et al. Inferring single-trial neural population dynamics using sequential auto-encoders. *Nature methods*, 15(10):805–815, 2018.
- Paszke, A., Gross, S., Massa, F., Lerer, A., Bradbury, J., Chanan, G., Killeen, T., Lin, Z., Gimelshein, N., Antiga, L., et al. Pytorch: An imperative style, high-performance deep learning library. *Advances in neural information processing systems*, 32, 2019.
- Payeur, A., Guergiev, J., Zenke, F., Richards, B. A., and Naud, R. Burst-dependent synaptic plasticity can coordinate learning in hierarchical circuits. *Nature neuroscience*, pp. 1–10, 2021.
- Perich, M. G., Arlt, C., Soares, S., Young, M. E., Mosher, C. P., Minxha, J., Carter, E., Rutishauser, U., Rudebeck, P. H., Harvey, C. D., et al. Inferring brain-wide interactions using data-constrained recurrent neural network models. *bioRxiv*, pp. 2020–12, 2021.
- Portes, J., Schmid, C., and Murray, J. M. Distinguishing learning rules with brain machine interfaces. *Advances in neural information processing systems*, 35:25937–25950, 2022.
- Pospisil, D. A., Larsen, B. W., Harvey, S. E., and Williams, A. H. Estimating shape distances on neural representations with limited samples. *arXiv preprint arXiv:2310.05742*, 2023.
- Raghu, M., Gilmer, J., Yosinski, J., and Sohl-Dickstein, J. Svcca: Singular vector canonical correlation analysis for deep learning dynamics and interpretability. *Advances in neural information processing systems*, 30, 2017.
- Remy, S. and Spruston, N. Dendritic spikes induce single-burst long-term potentiation. *Proceedings of the National Academy of Sciences*, 104(43):17192–17197, 2007.
- Richards, B. A., Lillicrap, T. P., Beaudoin, P., Bengio, Y., Bogacz, R., Christensen, A., Clopath, C., Costa, R. P., de Berker, A., Ganguli, S., et al. A deep learning framework for neuroscience. *Nature neuroscience*, 22(11):1761–1770, 2019.
- Roelfsema, P. R. and Holtmaat, A. Control of synaptic plasticity in deep cortical networks. *Nature Reviews Neuroscience*, 19(3):166–180, 2018.
- Sacramento, J., Costa, R. P., Bengio, Y., and Senn, W. Dendritic cortical microcircuits approximate the backpropagation algorithm. *arXiv preprint arXiv:1810.11393*, 2018.
- Salimans, T., Ho, J., Chen, X., Sidor, S., and Sutskever, I. Evolution strategies as a scalable alternative to reinforcement learning. *arXiv preprint arXiv:1703.03864*, 2017.
- Scellier, B. and Bengio, Y. Equilibrium propagation: Bridging the gap between energy-based models and backpropagation. *Frontiers in computational neuroscience*, 11:24, 2017.
- Schrimpf, M., Kubilius, J., Hong, H., Majaj, N. J., Rajalingham, R., Issa, E. B., Kar, K., Bashivan, P., Prescott-Roy, J., Geiger, F., et al. Brain-score: Which artificial neural network for object recognition is most brain-like? *BioRxiv*, 2018.
- Schuessler, F., Mastrogiossepe, F., Dubreuil, A., Ostojevic, S., and Barak, O. The interplay between randomness and structure during learning in rnns. *Advances in neural information processing systems*, 33:13352–13362, 2020.
- Schuessler, F., Mastrogiossepe, F., Ostojevic, S., and Barak, O. Aligned and oblique dynamics in recurrent neural networks. *arXiv preprint arXiv:2307.07654*, 2023.
- Sexton, N. J. and Love, B. C. Reassessing hierarchical correspondences between brain and deep networks through direct interface. *Science Advances*, 8(28), 2022.
- Shahbazi, M., Shirali, A., Aghajani, H., and Nili, H. Using distance on the riemannian manifold to compare representations in brain and in models. *NeuroImage*, 239:118271, 2021.
- Smith, S. J., Hawrylycz, M., Rossier, J., and Sümbül, U. New light on cortical neuropeptides and synaptic network plasticity. *Current Opinion in Neurobiology*, 63:176–188, aug 2020.
- Song, H. F., Yang, G. R., and Wang, X.-J. Training excitatory-inhibitory recurrent neural networks for cognitive tasks: a simple and flexible framework. *PLOS Computational Biology*, 12(2):1–30, 02 2016.
- Song, Y., Millidge, B., Salvatori, T., Lukasiewicz, T., Xu, Z., and Bogacz, R. Inferring neural activity before plasticity as a foundation for learning beyond backpropagation. *Nature Neuroscience*, 27(2):348–358, 2024.
- Sucholutsky, I., Muttenthaler, L., Weller, A., Peng, A., Bobu, A., Kim, B., Love, B. C., Grant, E., Achterberg, J., Tenenbaum, J. B., et al. Getting aligned on representational alignment. *arXiv preprint arXiv:2310.13018*, 2023.

- Sussillo, D. and Abbott, L. F. Generating coherent patterns of activity from chaotic neural networks. *Neuron*, 63(4): 544–557, 2009.
- Sussillo, D., Churchland, M. M., Kaufman, M. T., and Shenoy, K. V. A neural network that finds a naturalistic solution for the production of muscle activity. *Nature neuroscience*, 18(7):1025–1033, 2015.
- Turner, E., Dabholkar, K. V., and Barak, O. Charting and navigating the space of solutions for recurrent neural networks. *Advances in Neural Information Processing Systems*, 34:25320–25333, 2021.
- Valente, A., Ostojic, S., and Pillow, J. Probing the relationship between linear dynamical systems and low-rank recurrent neural network models. *arXiv preprint arXiv:2110.09804*, 2021.
- Von Oswald, J., Niklasson, E., Randazzo, E., Sacramento, J., Mordvintsev, A., Zhmoginov, A., and Vladymyrov, M. Transformers learn in-context by gradient descent. In *International Conference on Machine Learning*, pp. 35151–35174. PMLR, 2023.
- Vyas, S., Golub, M. D., Sussillo, D., and Shenoy, K. V. Computation through neural population dynamics. *Annual Review of Neuroscience*, 43:249–275, 2020.
- Wang, C., Dong, X., Jiang, J., Ji, Z., Liu, X., and Wu, S. Brainscale: Enabling scalable online learning in spiking neural networks. *bioRxiv*, pp. 2024–09, 2024.
- Werfel, J., Xie, X., and Seung, H. Learning curves for stochastic gradient descent in linear feedforward networks. *Advances in neural information processing systems*, 16, 2003.
- Williams, A. H., Kunz, E., Kornblith, S., and Linderman, S. Generalized shape metrics on neural representations. *Advances in Neural Information Processing Systems*, 34: 4738–4750, 2021.
- Woodworth, B., Gunasekar, S., Lee, J. D., Moroshko, E., Savarese, P., Golan, I., Soudry, D., and Srebro, N. Kernel and rich regimes in overparametrized models. In *Conference on Learning Theory*, pp. 3635–3673. PMLR, 2020.
- Xie, X. and Seung, H. S. Spike-based learning rules and stabilization of persistent neural activity. *Advances in neural information processing systems*, 12, 1999.
- Yamins, D. L., Hong, H., Cadieu, C. F., Solomon, E. A., Seibert, D., and DiCarlo, J. J. Performance-optimized hierarchical models predict neural responses in higher visual cortex. *Proceedings of the national academy of sciences*, 111(23):8619–8624, 2014.
- Yang, G. R. and Molano-Mazón, M. Towards the next generation of recurrent network models for cognitive neuroscience. *Current Opinion in Neurobiology*, 70:182–192, 2021.
- Yang, G. R. and Wang, X.-J. Artificial neural networks for neuroscientists: a primer. *Neuron*, 107(6):1048–1070, 2020.
- Yang, G. R., Joglekar, M. R., Song, H. F., Newsome, W. T., and Wang, X.-J. Task representations in neural networks trained to perform many cognitive tasks. *Nature neuroscience*, 22(2):297–306, 2019.
- Zador, A. M. A critique of pure learning and what artificial neural networks can learn from animal brains. *Nature communications*, 10(1):1–7, 2019.
- Zahorodnii, A., Mendoza-Halliday, D., Martinez-Trujillo, J. C., Qian, N., Desimone, R., and Cueva, C. J. Overcoming sensory-memory interference in working memory circuits. *bioRxiv*, pp. 2025–03, 2025.
- Zipser, D. Recurrent network model of the neural mechanism of short-term active memory. *Neural Computation*, 3(2):179–193, 1991.

A. Methods

A.1. Further Details on the Neural Datasets and Synthetic Data for RNN Training

The **Mante 2013** dataset was downloaded from <https://www.ini.uzh.ch/en/research/groups/mante/data.html>. We trained RNNs using a synthetic task setup from Neurogym (Molano-Mazon et al., 2022), which included a 350 ms fixation period, a 750 ms stimulus presentation period, a 300 ms delay period, and a 300 ms decision period. The activity of the trained RNNs during the stimulus period was then compared to the downloaded neural dataset using the aforementioned similarity measures. A grid search on the fixation and decision interval durations revealed only minor differences in distances and a consistent trend across learning rules.

The **Sussillo 2015** dataset consisted of electrode recordings from primary motor (M1) and dorsal premotor cortex (PMd) taken while a monkey performed a maze-reaching task consisting of 27 different reaching conditions (Sussillo et al., 2015). To assess the similarity between the neural activity and RNNs we compared activity from -1450 ms to 400 ms relative to movement onset. The inputs and outputs to train the models were described in Sussillo et al. 2015, but in brief, for each reach condition there were 16 inputs and 7 target outputs. The 7 outputs were the electromyographic (EMG) signals recorded from 7 muscles as the monkey performed a reaching movement. 15 inputs specified the upcoming reach condition, and were derived from preparatory period neural activity. The remaining input was a hold-cue that took a value of +1 before movement onset and then a value of 0 to initiate the movement, whereupon the model generated the 7 EMG signals.

A.2. Further Details on the Learning Rule

This subsection aims to clarify the approximation mechanisms employed by each bio-plausible learning rule. For comprehensive descriptions, we recommend consulting the detailed references provided. We begin by expressing the gradient via real-time recurrent learning (RTRL) factorization (an equivalent but causal alternative to the BPTT factorization of the gradient):

$$\frac{dL}{dW_{h,ij}} = \sum_{l,t} \frac{\partial L}{\partial h_{l,t}} \frac{dh_{l,t}}{dW_{h,ij}}, \quad (5)$$

We follow the total versus partial derivative notation (d vs. ∂) as in (Bellic et al., 2020). The primary challenge with RTRL in terms of biological plausibility and computational efficiency lies in the term $\frac{dh_{l,t}}{dW_{h,ij}}$ from the gradient decomposition (Eq. 5). This term tracks all recursive dependencies of $h_{l,t}$ on the weight $W_{h,ij}$ due to recurrent connections, calculated recursively as:

$$\begin{aligned} \frac{dh_{l,t}}{dW_{h,ij}} &= \frac{\partial h_{j,t}}{\partial W_{h,ij}} + \sum_m \frac{\partial h_{l,t}}{\partial h_{m,t-1}} \frac{dh_{m,t-1}}{dW_{h,ij}} \\ &= \frac{\partial h_{l,t}}{\partial W_{h,ij}} + \frac{\partial h_{l,t}}{\partial h_{l,t-1}} \frac{dh_{l,t-1}}{dW_{h,ij}} + \underbrace{\sum_{m \neq l} W_{h,lm} f'(h_{m,t-1}) \frac{dh_{m,t-1}}{dW_{h,ij}}}_{\text{involving all weights } W_{h,lm}}. \end{aligned} \quad (6)$$

Consequently, $\frac{dh_{l,t}}{dW_{h,ij}}$ presents a significant challenge for biological plausibility as it includes nonlocal terms, necessitating knowledge of all other network weights for updating each $W_{h,ij}$. **For a learning rule to be biologically plausible, all information required to update a synaptic weight must be physically accessible to that synapse. However, it remains unclear how neural circuits could make such extensive information readily available to every synapse.**

Approaches like **e-prop** (Bellic et al., 2020) and equivalently, **RFLO** (Murray, 2019), address this by truncating the problematic nonlocal terms in Eq. 6, ensuring that updates to $W_{h,ij}$ follow a three-factor framework — the updates rely solely on local pre- and post-synaptic activity and a third top-down instructive signal (e.g. from neuromodulators):

$$\widehat{\frac{\partial h_{l,t}}{\partial W_{h,ij}}} = \begin{cases} \frac{\partial h_{i,t}}{\partial W_{h,ij}} + \frac{\partial h_{i,t}}{\partial h_{i,t-1}} \widehat{\frac{\partial h_{i,t-1}}{\partial W_{h,ij}}}, & l = i \\ 0, & l \neq i \end{cases} \quad (7)$$

which yields a much simpler factor than the comprehensive tensor depicted in Eq. 6. This truncation can be achieved in PyTorch using `h.detach()`, preventing gradient propagation through the recurrent weights.

Putting this together, e-prop can be written in terms of known biological processes including — eligibility trace e and top-down instructive signals I — as (Bellec et al., 2020):

$$\Delta W_{h,ij}|_{e-prop} = \sum_t I_{i,t} e_{ij,t}, \quad (8)$$

where $I_{i,t} = \frac{\partial L}{\partial h_{i,t}}$ is the top-down instructive signal (e.g. from neuromodulator dopamine, neuronal firing, etc. (Gerstner et al., 2018; Bellec et al., 2020)) sent to neuron i at time t , and $e_{ij,t} = \widehat{\frac{\partial h_{i,t}}{\partial W_{h,ij}}} = \widehat{\frac{\partial h_{i,t}}{\partial W_{h,ij}}} + \widehat{\frac{\partial h_{i,t}}{\partial h_{i,t-1}}} \widehat{\frac{\partial h_{i,t-1}}{\partial W_{h,ij}}}$ is the eligibility trace for synapse (ij) at time t . This is a three-factor rule, with the pre-and postsynaptic neuron factors in the eligibility trace as well as a third factor from the instructive signal.

Besides eligibility traces and top-down instructive signals, recent transcriptomics data (Smith et al., 2020) suggest the presence of widespread cell-type-specific local modulatory signals that could convey additional information for guiding synaptic weight updates. **ModProp** is developed to incorporate these processes and restore the gradient terms truncated by e-prop, thereby improving the approximation of the gradient. Specifically, the ModProp update rule is described as follows (Liu et al., 2022b):

$$\begin{aligned} \Delta W_{h,ij}|_{ModProp} &\propto I_i \times e_{ij} + \left(\sum_{\alpha \in C} \left(\sum_{l \in \alpha} I_l h'_l \right) \times F_{\alpha\beta} \right) * e_{ij}, \\ F_{\alpha\beta,s} &= \mu^{s-1} (W^s)_{\alpha\beta}, \end{aligned} \quad (9)$$

where I and e again denote the top-down learning signal and the eligibility trace, respectively. Here, neuron j belongs to type α , neuron p to type β , and C denotes the set of cell types. $F_{\alpha\beta}$ is hypothesized to represent type-specific filter taps of GPCRs expressed by cells of type β in response to precursors secreted by cells of type α . The operator $*$ denotes convolution, and s indexes the filter taps. The hyperparameter μ , set to 0.25 in this study, and the genetically predetermined $(W^s)_{\alpha\beta}$ values for different filter taps $F_{\alpha\beta,s}$ could be optimized over evolutionary timescales (Liu et al., 2022b).

We also explored an older learning rule, **node perturbation** (Werfel et al., 2003; Lillicrap et al., 2016), which is known to have trouble scaling beyond small-scale networks and simple tasks. Specifically, it is implemented by

$$\Delta W_{h,ij}|_{NP} \propto \sum_t \widehat{I}_{i,t} e_{ij,t}, \quad (10)$$

where $\widehat{I}_t = (L_t(h_t + \xi) - L_t(h_t))\xi/\sigma^2$ provides an estimate to $\frac{\partial L}{\partial h_t}$; elements of ξ are chosen independently from a zero-mean Gaussian distribution with variance σ^2 .

In addition, we explored **evolutionary strategies** (Salimans et al., 2017) for parameter updates in our model. This method, for a Gaussian distribution, is implemented as follows:

$$\Delta W_{h,ij}|_{ES} \propto \frac{1}{\sigma S} \sum_{s=1}^S L^{(s)} \epsilon^{(s)}, \quad (11)$$

where $\epsilon^{(s)}$ is sampled from a standard normal distribution $\mathcal{N}(0, I)$ for $s = 1, \dots, S$. Here, $L^{(s)}$ represents the loss function evaluated after perturbing the parameter by $\sigma \epsilon^{(s)}$, σ is the standard deviation of the perturbations, and S is the number of samples. Due to computational constraints, we set S to 50 for our experiments.

A.3. Additional Details on Training and Analysis

Our model-data comparison method utilizes Procrustes distances, as implemented in <https://github.com/ahwillia/netrep>, with the configuration set to $metric = LinearMetric(alpha = 1.0, center_columns = True)$. Additionally, in Appendix Figure 8, we employed Dynamical Systems Analysis (DSA), available at <https://github.com/mitchelostrow/DSA/tree/main>. For this analysis, we tested with hyperparameters $n_delays \in \{5, 10, 15, 20\}$ and $rank \in \{10, 20, 30, 40\}$, observing consistent trends across settings. We did not test values beyond these ranges due to computational resource limitations. For the loss used in training RNNs, we used cross-entropy loss for the Mante 2013 task and mean-squared error for the Sussillo 2015 task (with EMG

outputs as the targets (Cloos et al., 2022)). As mentioned, the Mante 2013 dataset was downloaded from <https://www.ini.uzh.ch/en/research/groups/mante/data.html>. The Hatsopoulos 2007 dataset was downloaded from <https://datadryad.org/dataset/doi:10.5061/dryad.xsj3tx9cm>. However, we obtained the Sussillo 2015 dataset from the original authors and do not have permission to redistribute it.

Our code is available at <https://github.com/Helena-Yuhan-Liu/LearningRuleSimilarities/tree/main>. Both YHL and CJC contributed to the code development. We utilized PyTorch Version 1.10.2 (Paszke et al., 2019). Simulations were executed on a server equipped with two 20-core Intel(R) Xeon(R) CPU E5-2698 v4 at 2.20GHz. The average training duration for tasks was about 10 minutes, and the analysis pipeline required approximately 2 minutes per model. Training employed the Adam optimizer. Unless otherwise noted, the learning rate was set at $1e - 3$, optimized through a grid search of $\{3e - 3, 1e - 3, 3e - 4, 1e - 4\}$. We used a batch size of around 100; changes in this parameter led to negligible differences in the results. The number of time steps, T , for the Sussillo task was set to 186, matching the original data. The number of time steps T , for the Mante task was 34, based on $dt = 50$ ms from the original Mante paper and the total task duration in the Neurogym setting. Similar trends were observed when we varied dt and the durations of the fixation and delay periods. We employed 200 hidden units for the Sussillo 2015 task and 400 hidden units for the Mante 2013 task; doubling these numbers resulted in similar trends. Each simulation was repeated with four different seeds (except for 10 seeds for Figure 3B), and results for each seed were plotted as separate lines in our figures. Training involved 1000 SGD iterations for Sussillo 2015 and 3000 for Mante 2013, with input, recurrent, and readout weights all trainable. Local learning rule approximations were specifically applied to input and recurrent weights, due to the locality issues discussed in Section A.2. Unlike these weights, readout weights do not encounter such issues; hence, by default, the same readout weights were used for both forward and backward computations. However, as verified in Appendix Figure 10, employing random feedback readout weights for training (i.e., feedback alignment (Lillicrap et al., 2016)) resulted in comparable distances.

By default, zero-mean Gaussian noise with a standard deviation of 0.1 was added to the hidden activity, except in cases where the noise was removed to assess its impact. Typically, no connectivity constraints were applied, except for settings in Figure 7B where 80% of the neurons were enforced as strictly excitatory and 20% as inhibitory. To enforce Dale’s law, we used the same masking procedure in (Yang & Wang, 2020). Additionally, the Sussillo 2015 plot in Figure 1 applies a sparsity constraint, limiting only 25% of the recurrent weights to be nonzero and trainable. To initialize the weights, we initialized with random Gaussian distributions where each weight element $W_{h,i,j} \sim \mathcal{N}(0, g^2/N)$, with an initial weight variance of g ; unless otherwise mentioned, we set $g = 1.0$. Input and readout weights were initialized similarly as in (Yang & Wang, 2020) (see their *EIRNN.ipynb* notebook).

Normalized accuracy, which appears as the x-axis in several plots, is defined such that a value of 1 corresponds to perfect performance. For Sussillo 2015, normalized accuracy is calculated as $1 - \text{normalized mean squared error}$, as used in (DePasquale et al., 2018). In the case of Mante 2013, which involves a classification task where mean squared error is not applicable, normalized accuracy is computed as $1 - \text{cross entropy loss}$ to maintain consistency with the definition where 1 indicates the best performance. We also applied x-axis limits to constrain the range between 0 and 1 for uniformity. While we match task accuracies for neural similarity comparisons, we note that — as observed in prior work (Bellec et al., 2020) — e-prop typically requires more training iterations than BPTT to reach the same accuracy.

We detail the data-splitting procedure used for generating the noise floor, i.e. the baseline, in Figure 5. We split the neural data into nonoverlapping groups each containing N_{sample} neurons (*i*neurons1, *i*neurons2). We sample N_{sample} units from the RNN model (*i*units). We compute the distance between two samples of neural data $d_1 = D(i\text{neurons2}, i\text{neurons1})$. d_1 is the lowest we can hope to get given the variability in the neurons that were recorded. We compute the distance between samples of the model and neural data $d_2 = D(i\text{units}, i\text{neurons1})$. For each iteration of this procedure we get a new estimate for the distance between the model and data, and the data-to-data distance.

Number of trials averaged	1	5	10	15	20
Distance	0.513 ± 0.008	0.358 ± 0.005	0.280 ± 0.004	0.238 ± 0.003	0.212 ± 0.003

Table 4. Illustrating greater data-data distance when computed from single trials; note that these numbers are not comparable to those in Figure 5 due to different ways of subsampling.

Although the neural datasets used in this study contain multiple trials per condition, we did not compute data-data similarity via trial-based subsampling. This decision reflects the substantial trial-to-trial variability in single-trial firing

rate estimates, which can dominate the distance metric and obscure meaningful similarities—even between similar neural responses (Cunningham et al., 2009; Kay et al., 2024). As illustrated in Table A.3, data-data distances are substantially higher when computed from single trials, but decrease with trial averaging. This trend reflects how averaging across trials helps recover stable, condition-specific firing patterns. While existing methods (e.g., LFADS (Pandarinath et al., 2018)) have improved single-trial inference, accurate estimation of latent dynamics from single trials remains an open challenge. Therefore, following standard practice in systems neuroscience, we computed similarity based on trial-averaged responses. Our chosen data-data baseline (used in Figure 5) compares held-out subsets of neurons recorded under matched task conditions and timepoints, and serves to assess a practical question: if more neurons had been recorded from the same brain region, would they be distinguishable from model units?

B. Convergence and Divergence of E-prop Updates in a Toy Setting

We present the formal statement and proof for Proposition 4.1 in Proposition B.1.

Consider a 1-dimensional linear recurrent neural network (RNN) with a single scalar recurrent weight parameter W , input sequence $\{x_t\}_{t=1}^T \subset \mathbb{R}$, and output \hat{y} defined as the readout of the last hidden state h_T :

$$h_t = Wh_{t-1} + x_t, \quad \hat{y} = h_T, \quad (12)$$

leading to

$$\hat{y}(W) = \sum_{t=0}^{T-1} W^t x_{T-t}. \quad (13)$$

The loss function is the least-squares loss $L = \frac{1}{2}(\hat{y} - y)^2$. Assume a target $y = 0$, making $L = \frac{1}{2}\hat{y}^2$. We note that this simple setup effectively reduces to a polynomial root finding problem, with $\{x_t\}_{t=1}^T \subset \mathbb{R}$ as the coefficients. The corresponding gradient-based updates are modeled as a continuous-time dynamical system (CTDS), with specific forms for BPTT and e-prop updates:

$$\tau \frac{dW(t)}{dt} \Big|_{\text{BPTT}} = -\frac{dL}{dW} = -\hat{y}(W)\hat{y}'(W), \quad \tau \frac{dW(t)}{dt} \Big|_{\text{e-prop}} = -\hat{y}(W)x_{T-1}. \quad (14)$$

Proposition B.1. Consider the setup in Eqs. 12-14 and assume the polynomial $\hat{y}(W)$ has at least one real root W^* , where $\hat{y}(W^*) = 0$, and BPTT converges to W^* ; the Jacobian $J_{\text{e-prop}}(W)$ evaluated at W^* satisfies $\text{Re}(\lambda) < 0$, where λ is the eigenvalue of $J_{\text{e-prop}}(W^*)$; the input sequence $\{x_t\}_{t=1}^T$ satisfies $x_{T-1} \neq 0$, ensuring non-degenerate e-prop updates.

If $W(0)$ satisfies $\|W(0) - W^*\| < \delta$, where $\delta > 0$ is the radius of a neighborhood around W^* within which $\text{Re}(\lambda)$ of $J_{\text{e-prop}}(W) < 0$ for all W , requiring $\text{sign}(\hat{y}'(W)) = \text{sign}(x_{T-1})$ upon initialization, then the e-prop update will asymptotically converge to W^* . If $W(0)$ is initialized such that $\text{sign}(\hat{y}'(W)) = -\text{sign}(x_{T-1})$ and $\text{sign}(\hat{y}'(W(t))$ remains constant for $t \geq 0$, then e-prop will diverge.

Proof. We analyze the system governed by the e-prop updates as a continuous-time dynamical system (CTDS):

$$\tau \frac{dW(t)}{dt} = -\hat{y}(W)x_{T-1},$$

where the Jacobian is:

$$J_{\text{e-prop}}(W) = \frac{\partial}{\partial W} \left(\frac{dW(t)}{dt} \right) = -\frac{1}{\tau} \hat{y}'(W)x_{T-1}.$$

By definition, since $J_{\text{e-prop}}(W^*)$ is a scalar for 1-dimensional RNN, its eigenvalue is itself, and W^* is an asymptotically stable fixed point if and only if $J_{\text{e-prop}}(W^*) < 0$, ensuring that trajectories initialized sufficiently close to W^* converge to W^* .

We start by proving the existence of a case for convergence. Evaluate the Jacobian at W^* :

$$J_{\text{e-prop}}(W^*) = -\frac{1}{\tau} \hat{y}'(W^*)x_{T-1}.$$

Having $J_{\text{e-prop}}(W^*) < 0$ implies:

$$\hat{y}'(W^*)x_{T-1} > 0.$$

As provided in the Proposition statement, suppose $W(0)$ is initialized such that $\|W(0) - W^*\| < \delta$ for some $\delta > 0$ (within the asymptotic stability region of W^*), within which the Jacobian remains negative $J_{\text{e-prop}}(W(t)) < 0 \quad \forall t \geq 0$. In this region, the CTDS is a contracting flow:

$$\frac{d}{dt} \|W(t) - W^*\|^2 = 2(W(t) - W^*) \frac{dW(t)}{dt}.$$

Substitute the update rule:

$$\frac{d}{dt} \|W(t) - W^*\|^2 = -2 \frac{1}{\tau} (W(t) - W^*) \hat{y}(W(t)) x_{T-1}.$$

Using Taylor expansion near W^* , $\hat{y}(W(t)) \approx \hat{y}'(W^*)(W(t) - W^*)$. Thus:

$$\frac{d}{dt} \|W(t) - W^*\|^2 = -2\frac{1}{\tau}\hat{y}'(W^*)x_{T-1}(W(t) - W^*)^2.$$

Since $\hat{y}'(W^*)x_{T-1} > 0$, this ensures $\|W(t) - W^*\|^2$ decreases monotonically, proving convergence to W^* . As a side note, since $W(t)$ and W^* are scalars, $\|W(t) - W^*\|^2 = (W(t) - W^*)^2$.

We next prove the existence of a case for failure to converge. By the Proposition statement, if $W(0)$ is initialized such that $\text{sign}(\hat{y}'(W)) = -\text{sign}(x_{T-1})$, $\text{sign}(\hat{y}'(W(t)))$ remains constant for $t \geq 0$ and x_{T-1} is a constant, then

$$\hat{y}'(W)x_{T-1} < 0 \quad \forall t \geq 0.$$

This would imply that

$$J_{\text{e-prop}}(W(t)) > 0 \quad \forall t \geq 0.$$

Since the eigenvalue of Jacobian $J_{\text{e-prop}}(W(t))$ (i.e. itself, since J is a scalar here) has strictly positive real part for all $t \geq 0$ along the trajectory $W(t)$, $W(t)$ does not converge to any stable fixed point, including W^* .

□

To help visualize this theoretical result (facilitated by the simplicity of the polynomial root-finding setup), consider the following scenarios. For stable initialization, requiring the initialization to satisfy $\text{sign}(\hat{y}'(W)) = \text{sign}(x_{T-1})$ would mean that the trajectory begins on a rising edge when $\text{sign}(x_{T-1}) > 0$ or a falling edge when $\text{sign}(x_{T-1}) < 0$. For the unstable initialization case, requiring the initialization to satisfy $\text{sign}(\hat{y}'(W)) \neq \text{sign}(x_{T-1})$ would mean that the trajectory starts on an edge with mismatched signs, leading to initial divergence. However, if $\text{sign}(\hat{y}'(W(t)))$ changes during the trajectory (e.g., by entering a different region), the system may settle into a different basin of attraction; this scenario would violate the assumption of a constant $\text{sign}(\hat{y}'(W(t)))$ for all $t \geq 0$. A particular case of instability occurs when $\text{sign}(x_{T-1}) < 0$ at initialization and the trajectory is initialized on a far-right (or far-left) rising edge. Here, the weight updates diverge without entering any basin.

C. Additional Simulations

In Appendix Figure 6 displays the similarity among models in terms of their pairwise distances and their embeddings across different sampled training snapshots. In Appendix Figure 7, we demonstrate consistent patterns when recurrent noise is removed and Dale’s law is enforced. We also explore ModProp (Liu et al., 2022b), which incorporates cell-type-specific local modulatory signals to reintroduce terms omitted by e-prop; however, as ModProp is effective only under specific conditions (Dale’s law and *ReLU* activation), confining Appendix Figure 7B to these settings. Further analysis of post-training weight eigenspectrums and distances, conducted using Dynamical Similarity Analysis (DSA), reinforces the similarity between BPTT and e-prop, as shown in Appendix Figure 8.

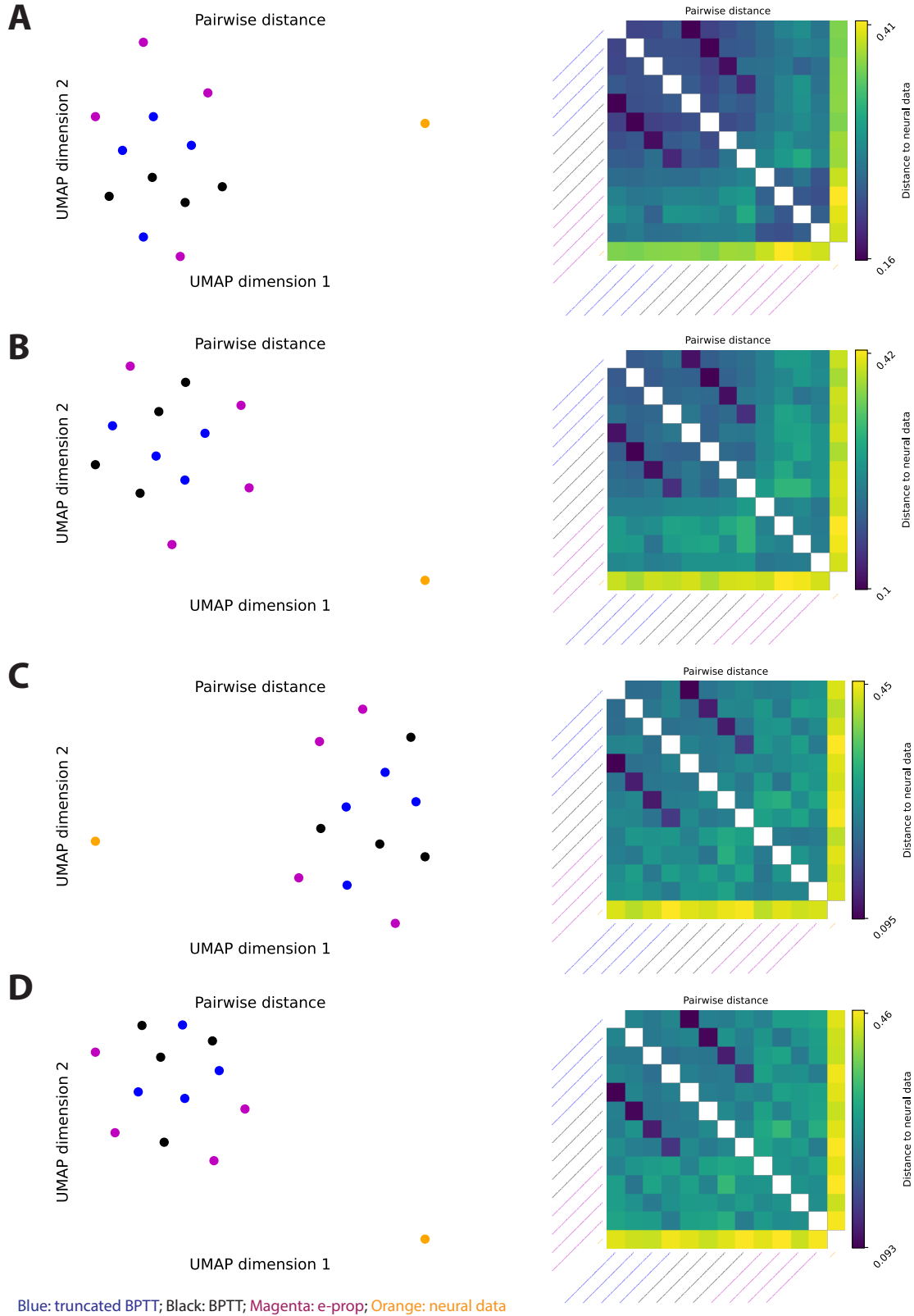


Figure 6. UMAP embedding and pairwise distance matrix heatmap for different models when (A) best e-prop accuracy, (B) 80%, (C) 60%, and (D) 40% accuracies are reached. Here, the Sussillo 2015 dataset is illustrated. Black: BPTT, blue: truncated BPTT, magenta: e-prop, orange: neural data. The pairwise distances show similarities across learning rules relative to data, indicated by lower distances between models as compared to model-data distance.

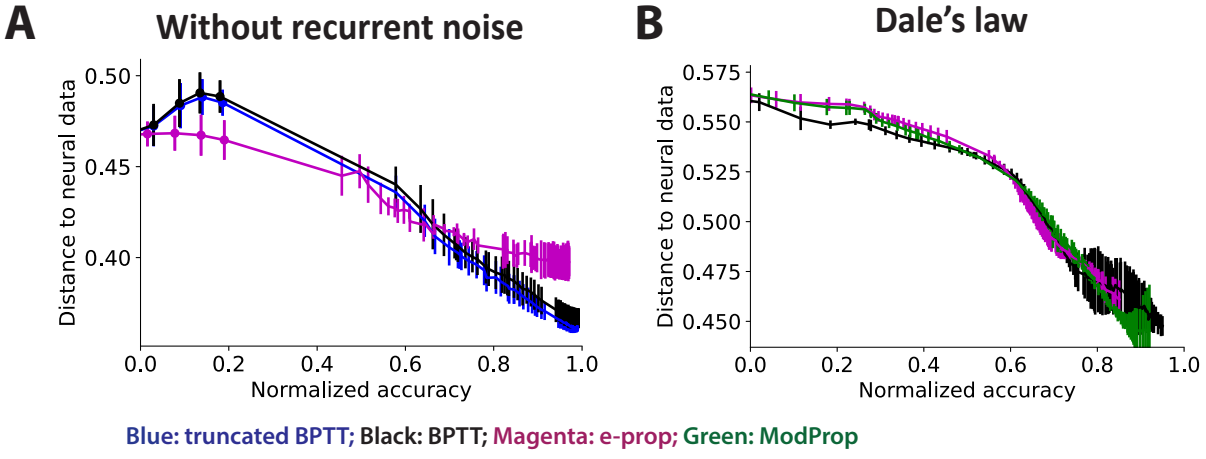


Figure 7. This figure replicates the core trend from Figure 1 — namely, comparable similarities across rules — under different settings. The settings include: (A) removal of RNN hidden activity noise, and (B) enforcement of Dale’s law. This plot uses the Sussillo2015 dataset as an illustrative example and compares Procrustes distances versus accuracy for three learning rules: BPTT (black), e-prop (magenta), and ModProp (green) — the latter functioning exclusively under Dale’s law constraint and *ReLU* activation. Plotting conventions mirroring those in Figure 1.

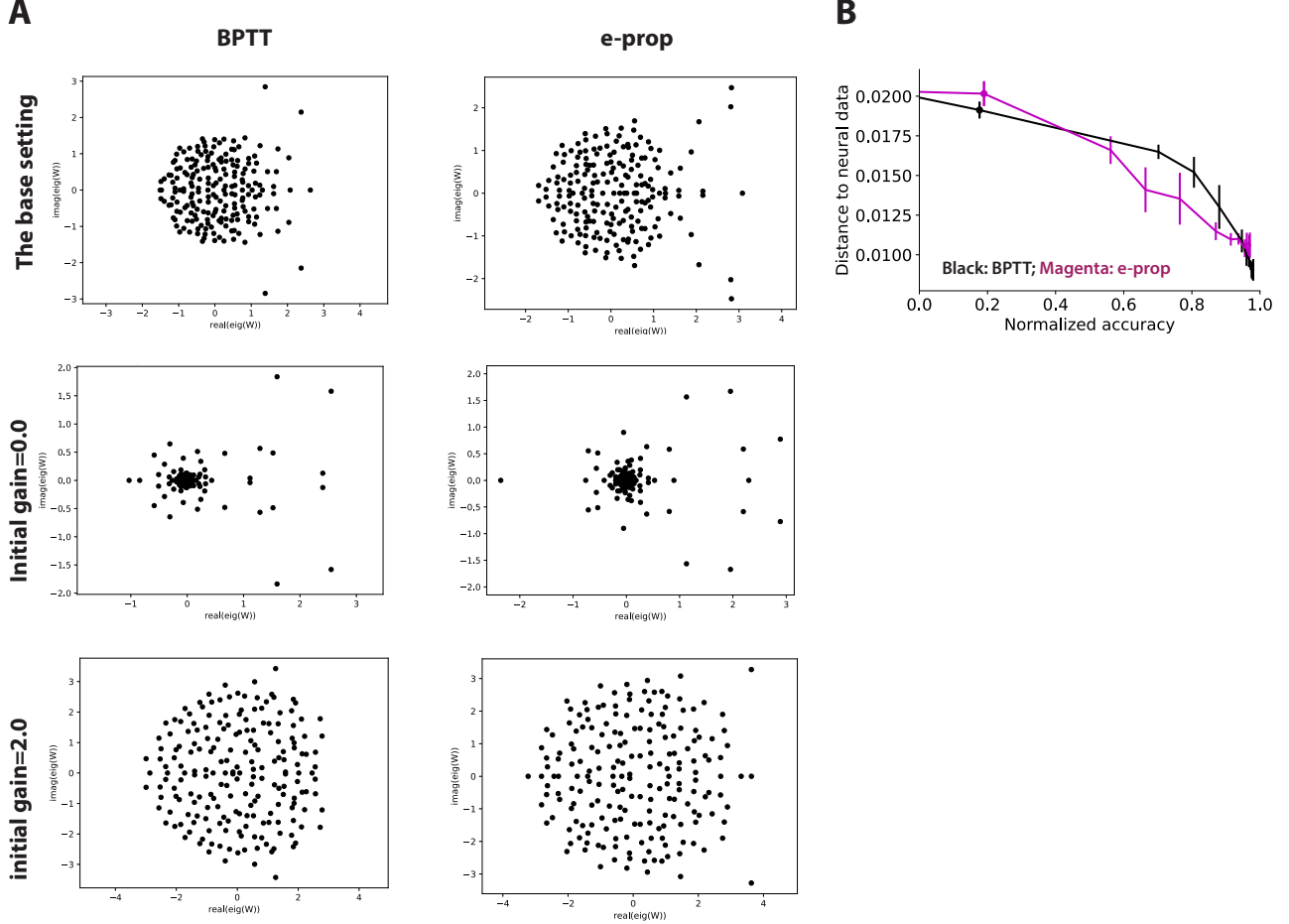


Figure 8. (A) presents the eigenvalues of the recurrent weight matrix post-training, with columns representing BPTT and e-prop respectively. Each row displays a different training setting: the base setting (referenced in Figure 1), initial weight standard deviation set to 0, and initial weight standard deviation set to $2/\sqrt{N}$. Notably, eigenvalue distributions appear more similar within each setting across learning rules (BPTT vs. e-prop) than across different settings for the same learning rule, further highlighting the similarity between BPTT and e-prop. B) The Dynamical Similarity Analysis (DSA), which evaluates systems based on their dynamical characteristics, is also unable to distinguish between learning rules when considering their proximity to neural data. Similar to previous figures, e-prop is plotted in magenta and BPTT is plotted in black.

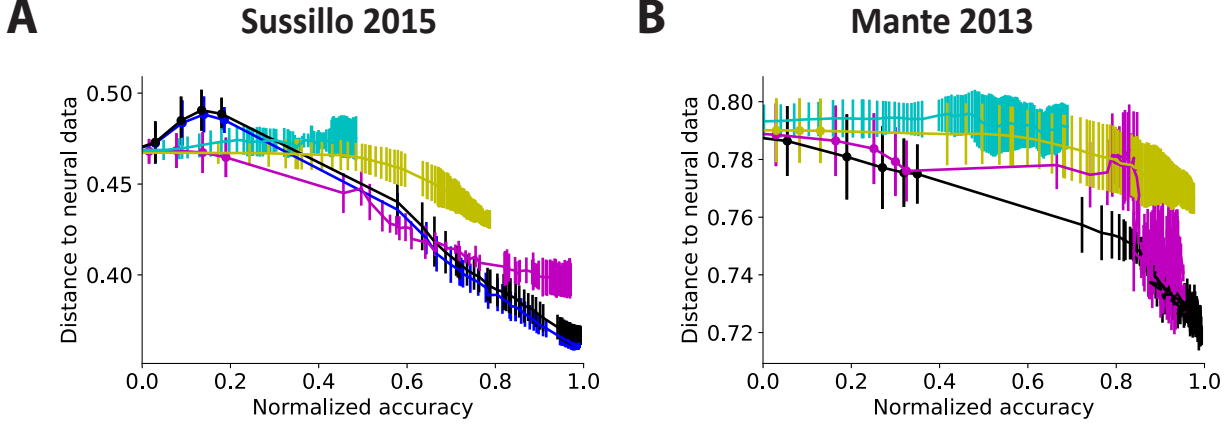


Figure 9. Node perturbation (cyan) and evolutionary strategies (yellow) lead to higher Procrustes distances from the neural data compared to BPTT (black) and e-prop (magenta) when accuracies are equivalent. This figure presents the Procrustes distance versus accuracy plots, adhering to the plotting conventions established in Figure 1, for (A) the Sussillo 2015 task and (B) the Mante 2013 task. Here, simulations are done without recurrent noise, as in Appendix Figure 7A, for a more stable performance of some learning rules.

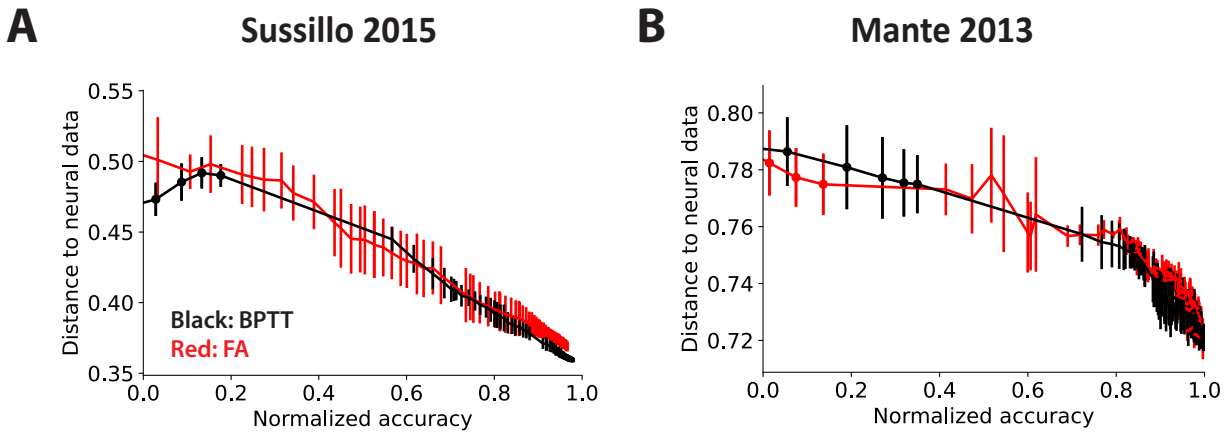


Figure 10. The use of random feedback readout weights for gradient computation (red) (Lillicrap et al., 2016) resulted in distances comparable to those achieved using exact readout weights (black). Plotting conventions are consistent with previous figures: task performance varies with training iterations, and error bars denote variation across seeds.